

A Joint Sparse Recovery Framework for Accurate Reconstruction of Inclusions in Elastic Media *

Jaejun Yoo^{†‡} Younghoon Jung^{†§} Mikyoung Lim^{§¶} Jong Chul Ye^{‡¶}
Abdul Wahab^{‡¶}

October 28, 2016

Abstract

We propose a robust algorithm to reconstruct the spatial support and the Lamé parameters of multiple inclusions in a homogeneous background elastic material using a few measurements of the displacement field over a finite collection of boundary points. The algorithm does not require any linearization or iterative update of Green's function, but still allows very accurate reconstruction. The breakthrough comes from a novel interpretation of Lippmann-Schwinger type integral representation of the displacement field in terms of unknown densities having common sparse support on the location of inclusions. Accordingly, the proposed algorithm consists of a two-step approach. First, the localization problem is recast as a joint sparse recovery problem that renders the densities and the inclusion support simultaneously. Then, a noise robust constrained optimization problem is formulated for the reconstruction of elastic parameters. An efficient algorithm is designed for numerical implementation using the Multiple Sparse Bayesian Learning (M-SBL) for joint sparse recovery problem and the Constrained Split Augmented Lagrangian Shrinkage Algorithm (C-SALSA) for the constrained optimization problem. The efficacy of the proposed framework is manifested through extensive numerical simulations. To the best of our knowledge, this is the first algorithm tailored for parameter reconstruction problems in elastic media using highly under-sampled data in the sense of Nyquist rate.

AMS subject classifications 2000. Primary: 35R30, 74B05, 74J20, 78A46. Secondary: 15A29, 45Q05, 65F50, 94A12

Key words. Elastic medium scattering, Elasticity imaging, Compressed sensing, Joint sparsity, Inverse scattering

*This research was supported by the Ministry of Science, ICT and Future Planning through the National Research Foundation of Korea grants NRF-2016R1A2B3008104 (to J.Y., J.C.Y., A.W.), NRF-2014R1A2A1A11052491 (to J.Y., J.C.Y., A.W.), NRF-2016R1A2B4014530 (to Y.J., M.L.), and NRF-2015H1D3A106240 (to A.W. through Korea Research Fellowship Program).

[†]J. Yoo and Y. Jung contributed equally to this work and are co-first authors.

[‡]Bio Imaging and Signal Processing Lab., Department of Bio and Brain Engineering, Korea Advanced Institute of Science and Technology, 291 Daehak-ro, Yuseong-gu, Daejeon 305-701, Korea (jaejun2004@kaist.ac.kr; jong.ye@kaist.ac.kr; wahab@kaist.ac.kr).

[§]Department of Mathematics, Korea Advanced Institute of Science and Technology, 291 Daehak-ro, Yuseong-gu, Daejeon 305-701, Korea (hapy1010@kaist.ac.kr; mklm@kaist.ac.kr).

[¶]Address all correspondence to A. Wahab at e-mail: wahab@kaist.ac.kr, Ph.:+82-42-350-4320, Fax:+82-42-350-4310. M. Lim and J. C. Ye are co-corresponding authors.

1 Introduction

Elasticity imaging or elastography is a set of thriving non-invasive imaging techniques that have led to significant improvements in the quantitative evaluation and visualization of mechanical properties of elastic materials [3, 29]. It aims to recover spatial variations in certain material and geometric parameters of structures inside an elastic body from displacement data obtained non-invasively over a part of the boundary surface or inside the body using classical imaging modalities such as ultrasound, magnetic resonance, or speckle interferometry [43, 45, 46, 47]. Different terminologies (static, quasi-static, time-harmonic, and dynamic elasticity imaging) are used to differentiate techniques based on excitation mechanism adopted to probe the underlying elastic body [44].

Elasticity imaging frameworks cater to a broad range of applications, for example, non-destructive testing of elastic objects for material impurities and structural integrity [25], exploration geophysics for mineral reservoir prospecting [48, 51], and medical diagnosis, in particular, for detection and characterization of potential tumors of diminishing sizes [45, 46, 43]. In the perspectives of medical diagnosis elasticity imaging aims to fathom spatial variations in the material parameters of human tissues by harnessing the interdependence between elastic field and tissue elasticity. It can be perceived as a modernization of tissue palpation technique to identify abnormalities that has been used for centuries [47]. In fact, the correlation between changes in the stiffness of tissues with pathological phenomena, such as cirrhosis of the liver [36], weakening of vessel walls and recruitment of collagen during tumorigenesis [27, 31, 52], has given an impetus to the quantitative characterization of underlying elastic properties using modern apparatus.

The inverse problem of quantitative evaluation of constitutive parameters is notorious for its complexity and ill-posed character. Many dedicated mathematical and computational algorithms for the reconstruction of location and parameters of anomalies of different geometrical nature (cavities, cracks and inclusions) have been proposed over the past few decades (see, for instance, [4, 9, 10, 11, 12, 20, 26, 28, 30, 32, 33, 25, 41, 42, 53], the survey articles [14, 15] and the monograph [3]). Most of the classical techniques are suited to continuous measurements, in other words, to experimental setups allowing to measure continuum deformations inside the elastic body or on a substantial part of its boundary. In practice, this requires mechanical systems that furnish discrete data sampled on a very fine grid conforming to Nyquist sampling rate, which is not practically feasible due to mechanical, computational and financial constraints. On the other hand, several algorithms are based on linearizations with respect to the leading order of the scale factor of inclusions (for instance, asymptotic expansion methods [4, 5]), or the variations in the constitutive parameters. Born, Rytov and Foldy-Lax type approximations are also adopted. These simplifications are not always valid and are too strong to allow an accurate reconstruction. This results in a dramatic loss of image resolution and quality. The algorithms avoiding such assumptions usually require iterative updates and only a handful of direct reconstruction algorithms can be found in the literature. Specifically, these techniques are computationally very costly and are highly prone to instabilities as they require computation of numerous forward solutions for iterative updates and suffer from intrinsic ill-posedness of the problem [40]. In a nutshell, the existing results found in the literature are clearly not satisfactory from practical view point.

In this work, we propose a novel and accurate imaging algorithm for the reconstruction of multiple inclusions present in a bounded isotropic homogeneous elastic formation. We assume that a few measurements of the displacement field over a small finite set of boundary points are available. For simplicity, we work in an elastostatic regime, however, the quasi-static and

time-harmonic elasticity problems are amenable to the same treatment with minor changes. One of the most important features of the proposed algorithm is that it does not require any linearization or iterative update of the Green's function; yet it is felicitous to furnish the spatial support of the inclusions and their material parameters very accurately. The breakthrough comes from a novel interpretation of Lippmann-Schwinger type integral representation of the displacement field that is derived in terms of unknown densities having jointly sparse spatial support on the location of inclusions. Therefore, the support identification problem can be recast as a joint sparse recovery problem for the unknown densities given that the support set of inclusions is itself sparse inside the elastic formation. This allows to invoke a variety of compressed sensing signal recovery algorithms. Consequently, using any one of these algorithms, the solution of this joint sparse recovery problem can be obtained which yields not only the spatial support of the inclusions but also renders the unknown densities. The Lamé parameters of the inclusions are estimated using recovered densities in the second step of the proposed imaging framework by solving a linear inverse problem in sought parameters.

It is worthwhile mentioning that the additional information contained in the recovered densities is linked to the perturbed displacement and strain fields inside the support of the inclusions. The availability of the internal data and the sparsity assumption on the support of inclusions thus compensate for the lack of over-determined measurements and significantly reduce the ill-posedness of the problem. In particular, this paves the way to a resolution enhancement since no linearization is applied in the proposed algorithm. Moreover, the numerical implementation of the proposed technique, as will be discussed later on in Section 5, does not require multiple forward solutions and is computationally very efficient. In fact, similar two-step approaches using joint sparse recovery formulation have been previously developed by our group for inverse scattering problems related to scalar Helmholtz equation [56], diffuse optical tomography [38, 39], and electric impedance tomography [37]. An extension to the electromagnetic inverse wave scattering governed by full Maxwell equations is on-going and has also provided very promising preliminary results. This extension will be reported elsewhere.

An important aspect of this work is the manifestation that even for elastic scattering problems, despite their complexity and ill-posedness, the derivation of an integral representation in terms of jointly sparse densities is possible that leads to an accurate and stable reconstruction with highly under-sampled data, which is not generally tractable by classical techniques. This clearly indicates, in view of the present investigation and the previously obtained results [56, 38, 39], that the proposed formulation may be so general that it provides a unified reconstruction framework for assorted inverse scattering problems.

The contents of this article are organized in the following order. The mathematical formulation of the inverse problem is provided in Section 2. The Lippmann-Schwinger type integral representation of the displacement field is derived in Section 3. Section 4 is dedicated to the joint sparse recovery based reconstruction algorithm. The computational aspects of the algorithm are discussed in Section 5. Several numerical experiments are conducted to substantiate the appropriateness of the proposed technique in Section 6. The article ends with a summary of this investigation and a brief discussion provided in Section 7.

2 Mathematical formulation

We specify in this section the nomenclature and assumptions that are adopted throughout this article and provide a mathematical formulation of the inverse problem dealt with in this article.

2.1 Preliminaries and nomenclature

Consider an open bounded domain $\Omega \subset \mathbb{R}^d$, $d = 2, 3$, with connected \mathcal{C}^2 -boundary $\partial\Omega$. Let us define $L^2(\Omega)$ as the space of square integrable functions in the usual way endowed with the norm

$$\|u\|_{L^2(\Omega)} := \left(\int_{\Omega} |u|^2 d\mathbf{x} \right)^{1/2}.$$

Let us define $H^1(\Omega)$ as the space of functions $u \in L^2(\Omega)$ such that $\partial_i u \in L^2(\Omega)$, for all $i \in \{1, \dots, d\}$, equipped with the norm

$$\|u\|_{H^1(\Omega)} := \left(\int_{\Omega} |u|^2 d\mathbf{x} + \int_{\Omega} |\nabla u|^2 d\mathbf{x} \right)^{1/2},$$

where the derivatives are implied in the weak sense. Moreover, $H^2(\Omega)$ and $H^{3/2}(\Omega)$ are defined respectively as the space of functions $u \in H^1(\Omega)$ such that $\partial_{ij} u \in L^2(\Omega)$, for all $i, j \in \{1, \dots, d\}$, and the interpolation space $[H^1(\Omega), H^2(\Omega)]_{1/2}$. The interested readers are referred, for instance, to the monograph by Bergh and Löfström [13] for further details.

To facilitate the latter analysis, we require the subspace $L^2_{\Psi}(\partial\Omega)$ of $L^2(\partial\Omega)^d$ defined by

$$L^2_{\Psi}(\partial\Omega) := \left\{ \boldsymbol{\varphi} \in L^2(\partial\Omega)^d \left| \int_{\partial\Omega} \boldsymbol{\varphi} \cdot \boldsymbol{\psi} d\sigma = 0, \quad \forall \boldsymbol{\psi} \in \Psi \right. \right\},$$

where Ψ is the $d(d+1)/2$ dimensional vector space of infinitesimal rigid displacements, that is,

$$\Psi := \left\{ \boldsymbol{\psi} \in H^1(\Omega)^d \left| \partial_i \psi_j + \partial_j \psi_i = 0, \quad 1 \leq i, j \leq d \right. \right\}.$$

It is interesting to note that the vector space Ψ contains constant functions and as a result

$$\int_{\partial\Omega} \boldsymbol{\varphi} d\sigma = 0, \quad \forall \boldsymbol{\varphi} \in L^2_{\Psi}(\partial\Omega).$$

Let Ω be loaded with an isotropic homogeneous elastic material so that its stiffness tensor $\mathbb{C}^0 = \left(C^0_{ijkl} \right)_{i,j,k,l=1}^d$ is defined by

$$C^0_{ijkl} := \lambda_0 \delta_{ij} \delta_{kl} + \mu_0 (\delta_{ik} \delta_{jl} + \delta_{il} \delta_{jk}),$$

where δ_{ij} is the Kronecker's delta function and constants λ_0 and μ_0 are respectively the compression and shear moduli of the elastic material. It is assumed that these Lamé parameters satisfy the conditions

$$\mu_0 > 0 \quad \text{and} \quad d\lambda_0 + 2\mu_0 > 0. \quad (2.1)$$

In fact, the conditions in (2.1) ensure the strong convexity of the stiffness tensor \mathbb{C}^0 . Precisely, for all symmetric matrices $\mathbf{A} \in \mathbb{R}^{d \times d} \setminus \{\mathbf{0}\}$, we have

$$(\mathbb{C}^0 : \mathbf{A}) : \mathbf{A} \geq \min(2\mu_0, d\lambda_0 + 2\mu_0) \|\mathbf{A}\|_F^2,$$

where the double dot operator “:” (with varying definitions for 2-, 3-, or 4-rank tensors by abuse of notation) and the Frobenius norm $\|\cdot\|_F$ are defined by

$$\mathbb{M} : \mathbf{A} := \left(\sum_{k,l=1}^d m_{ijkl} a_{kl} \right)_{i,j=1}^d, \quad \mathbf{A} : \mathbf{B} := \sum_{i,j=1}^d a_{ij} b_{ij} \quad \text{and} \quad \|\mathbf{A}\|_F := \sqrt{\mathbf{A} : \mathbf{A}}$$

for arbitrary real matrices $\mathbf{A} = (a_{ij})_{i,j=1}^d$, $\mathbf{B} = (b_{ij})_{i,j=1}^d$ and 4-rank tensors $\mathbb{M} = (m_{ijkl})_{i,j,k,l=1}^d$.

Suppose that the material loaded in Ω contains N open and bounded elastic inclusions D_n , $n = 1, \dots, N$, with simply connected smooth boundaries ∂D_n . To simplify the matters, we make the following assumptions throughout in this investigation.

- H1. All inclusions are separated apart from $\partial\Omega$ and their closures are mutually disjoint, that is, there exists a constant $d_0 \in \mathbb{R}_+$ such that

$$\inf_{x \in \overline{D_n}} \text{dist}(x, \partial\Omega) \geq d_0 \quad \text{and} \quad \inf_{x \in \overline{D_m}} \text{dist}(x, \overline{D_n}) \geq d_0, \quad \forall m \neq n,$$

where *dist* represents the usual distance function in \mathbb{R}^d .

- H2. Each D_n is isotropic but is allowed to be inhomogeneous so that its stiffness tensor

$$\mathbb{C}^n(\mathbf{x}) := \left(C_{ijkl}^n(\mathbf{x}) \right)_{i,j,k,l}^d \text{ is given by}$$

$$C_{ijkl}^n(\mathbf{x}) := \lambda_n(\mathbf{x}) \delta_{ij} \delta_{kl} + \mu_n(\mathbf{x}) (\delta_{ik} \delta_{jl} + \delta_{il} \delta_{jk}), \quad \forall \mathbf{x} \in D_n$$

in terms of spatially varying Lamé parameters $\lambda_n, \mu_n \in L^\infty(\Omega)$.

- H3. There exist constants $\underline{\lambda}_n, \bar{\lambda}_n, \underline{\mu}_n, \bar{\mu}_n \in \mathbb{R}$ such that

$$0 < \underline{\mu}_n \leq \mu_n(\mathbf{x}) \leq \bar{\mu}_n \quad \text{and} \quad 0 < d\underline{\lambda}_n + 2\underline{\mu}_n \leq d\lambda_n(\mathbf{x}) + 2\mu_n(\mathbf{x}) \leq d\bar{\lambda}_n + 2\bar{\mu}_n$$

for all $\mathbf{x} \in \overline{D_n}$ and $n \in \{1, \dots, N\}$. By this assumption, It is ensured that, for all symmetric matrices $\mathbf{A} \in \mathbb{R}^{d \times d} \setminus \{\mathbf{0}\}$ and $\mathbf{x} \in D_n$,

$$\max(2\bar{\mu}_n, d\bar{\lambda}_n + 2\bar{\mu}_n) \|\mathbf{A}\|_F^2 \geq (\mathbb{C}^n(\mathbf{x}) : \mathbf{A}) : \mathbf{A} \geq \min(2\underline{\mu}_n, d\underline{\lambda}_n + 2\underline{\mu}_n) \|\mathbf{A}\|_F^2.$$

- H4. We avoid the degenerate cases by assuming that, for all $n = 1, \dots, N$,

$$(\lambda_0 - \lambda_n(\mathbf{x}))^2 + (\mu_0 - \mu_n(\mathbf{x}))^2 \neq 0 \quad \text{and} \quad (\lambda_0 - \lambda_n(\mathbf{x}))(\mu_0 - \mu_n(\mathbf{x})) \geq 0, \quad \forall \mathbf{x} \in D_n.$$

In this way, it is also ensured that the stiffness tensor

$$\mathbb{C}^\star := \mathbb{C}^0 \chi[\Omega \setminus \cup_{n=1}^N \overline{D_n}] + \sum_{n=1}^N \mathbb{C}^n \chi[D_n]^*$$

of Ω in the presence of inclusions D_1, \dots, D_N also satisfies strong convexity condition. Here $\chi[D_n]$ represents the characteristic function of domain D_n .

To facilitate latter analysis, let us introduce piece-wise defined functions

$$\lambda(\mathbf{x}) := \sum_{n=1}^N \lambda_n(\mathbf{x}) \chi[D_n](\mathbf{x}), \quad \mu(\mathbf{x}) := \sum_{n=1}^N \mu_n(\mathbf{x}) \chi[D_n](\mathbf{x}), \quad \mathbb{C}(\mathbf{x}) := \sum_{n=1}^N \mathbb{C}^n(\mathbf{x}) \chi[D_n](\mathbf{x})$$

for all $\mathbf{x} \in \cup_{n=1}^N D_n$. We shall adopt following conventions henceforth. Let $\mathbf{p} = (p_i)_{i=1}^d$, $\mathbf{A} = (a_{ij})_{i,j=1}^d$ and $\mathbf{B} = (b_{ijk})_{i,j,k=1}^d$ be respectively arbitrary vector, matrix and 3-rank tensor.

Let $\mathbf{H} : \mathbb{R}^d \rightarrow H^1(\Omega)^{d \times d}$, $\mathbf{x} \mapsto (h_{ij}(\mathbf{x}))_{i,j=1}^d$ be any matrix valued function and $(\hat{\mathbf{e}}_1, \dots, \hat{\mathbf{e}}_d)$ be the standard basis in \mathbb{R}^d . Then

$$\begin{aligned} \mathbf{A} \cdot \mathbf{p} &:= \sum_{i,j=1}^d a_{ij} p_j \hat{\mathbf{e}}_i, & \mathbf{B} : \mathbf{A} &:= \sum_{i,j,k=1}^d b_{ijk} a_{jk} \hat{\mathbf{e}}_i, & \nabla \cdot \mathbf{H}(\mathbf{x}) &:= \sum_{i,j=1}^d \left(\frac{\partial h_{ij}}{\partial x_i}(\mathbf{x}) \right) \hat{\mathbf{e}}_j, \\ [\nabla \mathbf{H}(\mathbf{x})]_{ijk} &:= \frac{\partial h_{ij}}{\partial x_k}(\mathbf{x}), & [(\nabla \mathbf{H}(\mathbf{x}))^\top]_{ijk} &:= \frac{\partial h_{ik}}{\partial x_j}(\mathbf{x}), & \forall i, j, k \in \{1, \dots, d\}, \end{aligned}$$

where superposed \top indicates transpose and the notation $[\cdot]$ is used to denote a component of a tensor, matrix or vector (e.g. for vector \mathbf{p} we have $[\mathbf{p}]_i = p_i$). Moreover, we define operator $\text{slice}_1 : \{1, \dots, d\} \times \mathbb{R}^{d \times d \times d} \rightarrow \mathbb{R}^{d \times d}$ and $\text{vec} : \mathbb{R}^{d \times d} \rightarrow \mathbb{R}^{d^2}$ by

$$\text{slice}_1(i, \mathbf{B}) := (b_{ijk})_{j,k=1}^d \quad (\text{for fixed } i) \quad \text{and} \quad \text{vec}(\mathbf{A}) := (\mathbf{a}_1^\top, \dots, \mathbf{a}_d^\top)^\top,$$

where \mathbf{a}_i denotes the i -th column of matrix \mathbf{A} .

2.2 Problem formulation

Let $\mathbf{u}_m : \bar{\Omega} \rightarrow \mathbb{R}^d$, for $m = 1, \dots, M \in \mathbb{N}$, be the displacement field in Ω , in the presence of D_1, \dots, D_N , caused by an applied surface traction $\mathbf{g}_m \in L_\Psi^2(\partial\Omega)$ on its boundary $\partial\Omega$. Then the vector field \mathbf{u}_m is the solution to

$$\begin{cases} \nabla \cdot (\mathbb{C}^* : \mathcal{E}[\mathbf{u}_m]) = \mathbf{0} & \text{in } \Omega \\ (\mathbb{C}^0 : \mathcal{E}[\mathbf{u}_m]) \cdot \boldsymbol{\nu} = \mathbf{g}_m & \text{on } \partial\Omega, \end{cases} \quad (2.2)$$

where $\mathbf{u}_m \in H^1(\Omega)$ such that $\mathbf{u}_m|_{\partial\Omega} \in L_\Psi^2(\partial\Omega)$ in order to ensure the existence of a unique weak solution. Here $\boldsymbol{\nu}$ is the outward unit normal to $\partial\Omega$ and $\mathcal{E}(\mathbf{u}_m)$ denotes the strain tensor related to \mathbf{u}_m given by $\mathcal{E}[\mathbf{u}_m] := (\nabla \mathbf{u}_m + \nabla \mathbf{u}_m^\top)/2$.

For convenience, we will usually denote the linear isotropic elasticity operator and the corresponding surface traction associated with \mathbb{C}^0 by $\mathcal{L}_{\lambda_0, \mu_0}$ and $\partial/\partial \boldsymbol{\nu}$ respectively, that is, for any smooth function $\mathbf{w} : \mathbb{R}^d \rightarrow \mathbb{R}^d$ we define

$$\begin{aligned} \mathcal{L}_{\lambda_0, \mu_0}[\mathbf{w}] &:= \nabla \cdot (\mathbb{C}^0 : \mathcal{E}[\mathbf{w}]) \\ \frac{\partial \mathbf{w}}{\partial \boldsymbol{\nu}} &:= (\mathbb{C}^0 : \mathcal{E}[\mathbf{w}]) \cdot \boldsymbol{\nu} = \lambda_0 (\nabla \cdot \mathbf{w}) \boldsymbol{\nu} + 2\mu_0 \mathcal{E}(\mathbf{w}) \cdot \boldsymbol{\nu}. \end{aligned}$$

Similarly, we will use analogous notation $\mathcal{L}_{\lambda, \mu}$ and $\partial/\partial \tilde{\boldsymbol{\nu}}$ corresponding to \mathbb{C} (i.e. to λ and μ). We will use a *de facto* extension of these operators for matrix valued functions using conventions listed in Subsection 2.1.

It can be easily verified that the problem (2.2) is equivalent to the transmission problem

$$\begin{cases} \mathcal{L}_{\lambda_0, \mu_0}[\mathbf{u}_m] = 0 & \text{in } \Omega \setminus \cup_{n=1}^N \overline{D_n} \\ \mathcal{L}_{\lambda, \mu}[\mathbf{u}_m] = 0 & \text{in } \cup_{n=1}^N D_n \\ \mathbf{u}_m|_- = \mathbf{u}_m|_+ & \text{on } \partial D_n \quad (\forall n = 1, \dots, N) \\ \frac{\partial \mathbf{u}_m}{\partial \tilde{\boldsymbol{\nu}}}|_- = \frac{\partial \mathbf{u}_m}{\partial \boldsymbol{\nu}}|_+ & \text{on } \partial D_n \quad (\forall n = 1, \dots, N) \\ \frac{\partial \mathbf{u}_m}{\partial \boldsymbol{\nu}} = \mathbf{g}_m & \text{on } \partial\Omega \quad \left(\mathbf{u}_m|_{\partial\Omega} \in L_\Psi^2(\partial\Omega) \right), \end{cases} \quad (2.3)$$

where subscripts $+$ and $-$ indicate the limiting values across the interface ∂D_n from outside and from inside D_n respectively, that is, for any function \mathbf{w}

$$\mathbf{w}(\mathbf{x})|_{\pm} := \lim_{\epsilon \rightarrow 0^+} \mathbf{w}(\mathbf{x} \pm \epsilon \boldsymbol{\nu}), \quad \mathbf{x} \in \partial D_n.$$

We also require the background displacement field \mathbf{U}_m in Ω (in the absence of any inclusion) caused by the surface traction $\mathbf{g}_m \in L^2_{\Psi}(\partial\Omega)$ applied on $\partial\Omega$. The vector field $\mathbf{U}_m : \bar{\Omega} \rightarrow \mathbb{R}^d$ is the solution to

$$\begin{cases} \mathcal{L}_{\lambda_0, \mu_0}[\mathbf{U}_m] = 0 & \text{in } \Omega \\ \frac{\partial \mathbf{U}_m}{\partial \boldsymbol{\nu}} = \mathbf{g}_m & \text{on } \partial\Omega \quad \left(\mathbf{U}_m|_{\partial\Omega} \in L^2_{\Psi}(\partial\Omega) \right). \end{cases}$$

We are now fully prepared to introduce the inverse problem dealt with in this article.

Inverse Problem

Let $\{\mathbf{x}_r\}_{r=1}^R \subset \partial\Omega$, for some $R \in \mathbb{N}$, be a finite collection of points on $\partial\Omega$. Let a known traction $\mathbf{g}_m \in L^2_{\Psi}(\partial\Omega)$, for each $m \in \{1, \dots, M \in \mathbb{N}\}$, be applied on $\partial\Omega$ which induces the displacement fields \mathbf{u}_m and \mathbf{U}_m in Ω respectively with and without the presence of inclusions D_1, \dots, D_N . Then, given the set of measurements

$$\left\{ (\mathbf{u}_m - \mathbf{U}_m)(\mathbf{x}_r) \mid r = 1, \dots, R, m = 1, \dots, M \right\},$$

locate inclusions D_1, \dots, D_N and reconstruct the corresponding Lamé parameters λ_n and μ_n for all $n = 1, \dots, N$. \square

3 Lippmann-Schwinger type integral form of perturbed displacement

The main ingredient of our reconstruction framework is a Lippmann-Schwinger type integral representation of the perturbations in the displacement fields, $\mathbf{u}_m - \mathbf{U}_m$, due to the presence of inclusions D_1, \dots, D_N . In this section, we derive an exact analytic formula for the perturbations $\mathbf{u}_m - \mathbf{U}_m$ using tools mostly borrowed from the existing literature on integral equations. Towards this end, we feel it best to pause and recall a few elements from layer potential theory for linear elastostatic system in the next subsection. The readers interested in further details are invited to read, for instance, the recent monograph [3].

3.1 Elements of layer potential theory for elastostatics

Let $\boldsymbol{\Gamma}$ denote the Kelvin matrix of fundamental solutions to the elastostatic system $\mathcal{L}_{\lambda_0, \mu_0}$ in \mathbb{R}^d , that is,

$$\mathcal{L}_{\lambda_0, \mu_0}[\boldsymbol{\Gamma}](\mathbf{x}) = -\delta_0(\mathbf{x})\mathbf{I}_d, \quad \forall \mathbf{x} \in \mathbb{R}^d,$$

where $\mathbf{I}_d \in \mathbb{R}^{d \times d}$ is the identity matrix and δ_0 is the Dirac mass at $\mathbf{0}$. It is well known that (see, for instance, [6, Lemma 6.2])

$$\boldsymbol{\Gamma}(\mathbf{x}) = \begin{cases} \alpha \ln |\mathbf{x}| \mathbf{I}_2 - \frac{\beta}{|\mathbf{x}|^2} \mathbf{x} \mathbf{x}^\top & \text{for } d = 2 \\ -\frac{\alpha}{2|\mathbf{x}|} \mathbf{I}_3 + \frac{\beta}{2|\mathbf{x}|^3} \mathbf{x} \mathbf{x}^\top & \text{for } d = 3, \end{cases}$$

where the parameters α and β are given by

$$\alpha := \frac{\lambda_0 + 3\mu_0}{4\pi\mu_0(\lambda_0 + 2\mu_0)} \quad \text{and} \quad \beta := \frac{\lambda_0 + \mu_0}{4\pi\mu_0(\lambda_0 + 2\mu_0)}. \quad (3.1)$$

Then the double layer potential \mathcal{D}_Ω associated with operator $\mathcal{L}_{\lambda_0, \mu_0}$ in Ω is defined by

$$\mathcal{D}_\Omega[\varphi](\mathbf{x}) := \int_{\partial\Omega} \frac{\partial}{\partial \nu_{\mathbf{y}}} \mathbf{\Gamma}(\mathbf{x} - \mathbf{y}) \cdot \varphi(\mathbf{y}) d\sigma(\mathbf{y}), \quad \mathbf{x} \in \mathbb{R}^d \setminus \partial\Omega$$

for all $\varphi \in L^2(\partial\Omega)^d$. Here $d\sigma$ denotes the infinitesimal surface element on $\partial\Omega$. We remind that $\mathcal{D}_\Omega[\varphi]$ is a solution to $\mathcal{L}_{\lambda_0, \mu_0}[\mathcal{D}_\Omega[\varphi]] = \mathbf{0}$ in $\mathbb{R}^d \setminus \partial\Omega$ for all $\varphi \in L^2_\Psi(\partial\Omega)$ and the quantities $\mathcal{D}_\Omega[\varphi]|_\pm$ are well-defined for all $\mathbf{x} \in \partial\Omega$. In fact, following jump relations hold (see [22])

$$\mathcal{D}_\Omega[\varphi]|_\pm(\mathbf{x}) = \left(\mp \frac{1}{2} \mathcal{I} + \mathcal{K}_\Omega \right) \varphi(\mathbf{x}) \quad \text{a.e.} \quad \mathbf{x} \in \partial\Omega, \quad (3.2)$$

where $\mathcal{I} : L^2(\partial\Omega)^d \rightarrow L^2(\partial\Omega)^d$ is the identity map and \mathcal{K}_Ω is a *Neumann-Poincaré operator* defined by

$$\mathcal{K}_\Omega[\varphi](\mathbf{x}) := \text{p.v.} \int_{\partial\Omega} \frac{\partial}{\partial \nu_{\mathbf{y}}} \mathbf{\Gamma}(\mathbf{x} - \mathbf{y}) \cdot \varphi(\mathbf{y}) d\sigma(\mathbf{y}), \quad \text{a.e.} \quad \mathbf{x} \in \partial\Omega$$

for all $\varphi \in L^2(\partial\Omega)^d$. Here *p.v.* stands for Cauchy principle value.

Let $\mathbf{N}(\cdot, \mathbf{y}) : \overline{\Omega} \rightarrow \mathbb{R}^{d \times d}$, for a fixed $\mathbf{y} \in \overline{\Omega}$, be the Neumann function for the background domain Ω without any inclusion, that is, the weak solution to

$$\begin{cases} \mathcal{L}_{\lambda_0, \mu_0}[\mathbf{N}](\mathbf{x}, \mathbf{y}) = -\delta_{\mathbf{y}}(\mathbf{x}) \mathbf{I}_d & \text{for } \mathbf{x} \in \Omega \\ \frac{\partial \mathbf{N}}{\partial \nu}(\mathbf{x}, \mathbf{y}) = -\frac{1}{|\partial\Omega|} \mathbf{I}_d & \text{for } \mathbf{x} \in \partial\Omega \end{cases} \quad (3.3)$$

subject to normalization condition

$$\int_{\partial\Omega} \mathbf{N}(\mathbf{x}, \mathbf{y}) \cdot \boldsymbol{\psi}(\mathbf{x}) d\sigma(\mathbf{x}) = \mathbf{0}, \quad \forall \boldsymbol{\psi} \in \Psi.$$

The following result from [6, Lemma 6.16] is of great significance in the latter analysis.

Lemma 3.1. *For all $\mathbf{x} \in \partial\Omega$ and $\mathbf{y} \in \Omega$*

$$\left(-\frac{1}{2} I + \mathcal{K}_\Omega \right) [\mathbf{N}(\cdot, \mathbf{y})](\mathbf{x}) = \mathbf{\Gamma}(\mathbf{x}, \mathbf{y}) \quad \text{modulo } \Psi.$$

Lemma 3.1 indicates that the operator $(-\mathcal{I}/2 + \mathcal{K}_\Omega)$ *filters* the effects of an imposed traction condition and maps the solution of the elastostatic system in Ω with traction condition on $\partial\Omega$ to a solution of elastostatic system in \mathbb{R}^d . The operator $(-\mathcal{I}/2 + \mathcal{K}_\Omega)$ will be coined as Calderón preconditioner in the sequel and will be effectively used in this article to design an efficient reconstruction algorithm.

3.2 Integral representation of perturbed displacement field

To facilitate the ensuing analysis, we feel it best to recall the Green's identities corresponding to elastostatic system beforehand. These identities can be easily derived using integration by parts and the divergence theorem (see, for instance, [6, Sec. 9.1]).

1. If $\mathbf{v} \in H^1(\Omega)^d$ and $\mathbf{w} \in H^{3/2}(\Omega)^d$ then

$$\int_{\partial\Omega} \mathbf{v} \cdot \frac{\partial \mathbf{w}}{\partial \boldsymbol{\nu}} d\sigma = \int_{\Omega} \mathbf{v} \cdot \mathcal{L}_{\lambda_0, \mu_0}[\mathbf{w}] d\mathbf{x} + \mathcal{Q}_{\Omega}^{\mathbb{C}^0}(\mathbf{v}, \mathbf{w}), \quad (3.4)$$

where the quadratic form $\mathcal{Q}_{\Omega}^{\mathbb{C}^0} : H^1(\Omega)^d \times H^1(\Omega)^d \rightarrow \mathbb{R}$ is defined by

$$\mathcal{Q}_{\Omega}^{\mathbb{C}^0}(\mathbf{v}, \mathbf{w}) := \int_{\Omega} \mathcal{E}[\mathbf{v}] : \mathbb{C}^0 : \mathcal{E}[\mathbf{w}] d\mathbf{x} = \int_{\Omega} \left[\lambda_0 (\nabla \cdot \mathbf{v})(\nabla \cdot \mathbf{w}) + 2\mu_0 (\mathcal{E}[\mathbf{v}] : \mathcal{E}[\mathbf{w}]) \right] d\mathbf{x}.$$

We shall use the *de facto* extension of $\mathcal{Q}_{\Omega}^{\mathbb{C}^0}$ if one of the arguments is a matrix, in which case it would yield a vector output.

2. If $\mathbf{v}, \mathbf{w} \in H^{3/2}(\Omega)^d$ then the formula (3.4) furnishes another Green's identity

$$\int_{\partial\Omega} \left(\mathbf{v} \cdot \frac{\partial \mathbf{w}}{\partial \boldsymbol{\nu}} - \mathbf{w} \cdot \frac{\partial \mathbf{v}}{\partial \boldsymbol{\nu}} \right) d\sigma(\mathbf{x}) = \int_{\Omega} (\mathbf{v} \cdot \mathcal{L}_{\lambda_0, \mu_0}[\mathbf{w}] - \mathbf{w} \cdot \mathcal{L}_{\lambda_0, \mu_0}[\mathbf{v}]) d\mathbf{x}. \quad (3.5)$$

It is interesting to note by formula (3.5) that if \mathbf{v} is in addition a solution to $\mathcal{L}_{\lambda_0, \mu_0}[\mathbf{v}] = \mathbf{0}$ in Ω then $\partial \mathbf{v} / \partial \boldsymbol{\nu} \in L_{\Psi}^2(\partial\Omega)$.

Let us now derive the integral representation of the perturbed displacement field. We start with the representation

$$\mathbf{U}_m(\mathbf{x}) = \int_{\partial\Omega} \mathbf{N}(\mathbf{x}, \mathbf{y}) \cdot \mathbf{g}_m(\mathbf{y}) d\sigma(\mathbf{y}) = \int_{\partial\Omega} \mathbf{N}(\mathbf{x}, \mathbf{y}) \cdot \frac{\partial \mathbf{u}_m}{\partial \boldsymbol{\nu}}(\mathbf{y}) d\sigma(\mathbf{y}), \quad \mathbf{x} \in \overline{\Omega}$$

of the background solution \mathbf{U}_m . Note that, by virtue of the imposed boundary condition on \mathbf{N} and the fact that $\mathbf{u}_m|_{\partial\Omega} \in L_{\Psi}^2(\partial\Omega)$, we have

$$\int_{\partial\Omega} \frac{\partial}{\partial \boldsymbol{\nu}_{\mathbf{y}}} \mathbf{N}(\mathbf{x}, \mathbf{y}) \cdot \mathbf{u}_m(\mathbf{y}) d\sigma(\mathbf{y}) = \mathbf{0}, \quad \mathbf{x} \in \overline{\Omega}.$$

Therefore, the background field can be expressed as

$$\mathbf{U}_m(\mathbf{x}) = \int_{\partial\Omega} \left(\mathbf{N}(\mathbf{x}, \mathbf{y}) \cdot \frac{\partial \mathbf{u}_m}{\partial \boldsymbol{\nu}}(\mathbf{y}) - \frac{\partial}{\partial \boldsymbol{\nu}_{\mathbf{y}}} \mathbf{N}(\mathbf{x}, \mathbf{y}) \cdot \mathbf{u}_m(\mathbf{y}) \right) d\sigma(\mathbf{y}), \quad \mathbf{x} \in \overline{\Omega}.$$

Consequently, a simple application of the Green's formula (3.5) over $\Omega \setminus \cup_{n=1}^N \overline{D_n}$ furnishes

$$\begin{aligned} \mathbf{U}_m(\mathbf{x}) = & - \int_{\Omega \setminus \cup_{n=1}^N \overline{D_n}} \left(\mathcal{L}_{\lambda_0, \mu_0}[\mathbf{N}](\mathbf{x}, \mathbf{y}) \cdot \mathbf{u}_m(\mathbf{y}) - \mathbf{N}(\mathbf{x}, \mathbf{y}) \cdot \mathcal{L}_{\lambda_0, \mu_0}[\mathbf{u}_m](\mathbf{y}) \right) d\mathbf{y} \\ & + \sum_{n=1}^N \int_{\partial D_n} \left(\mathbf{N}(\mathbf{x}, \mathbf{y}) \cdot \frac{\partial \mathbf{u}_m}{\partial \boldsymbol{\nu}}(\mathbf{y}) \Big|_+ - \frac{\partial}{\partial \boldsymbol{\nu}_{\mathbf{y}}} \mathbf{N}(\mathbf{x}, \mathbf{y}) \cdot \mathbf{u}_m(\mathbf{y}) \Big|_+ \right) d\sigma(\mathbf{y}), \quad \mathbf{x} \in \overline{\Omega}. \end{aligned} \quad (3.6)$$

Remark that the second term on the right hand side (RHS) of (3.6) is identically zero thanks to the first equation in (2.3). Moreover, by invoking the transmission conditions on the displacement \mathbf{u}_m and its surface traction on the boundaries ∂D_n in (2.3) one obtains

$$\begin{aligned} \mathbf{U}_m(\mathbf{x}) = & - \int_{\Omega \setminus \cup_{n=1}^N \overline{D_n}} \mathcal{L}_{\lambda_0, \mu_0}[\mathbf{N}](\mathbf{x}, \mathbf{y}) \cdot \mathbf{u}_m(\mathbf{y}) d\mathbf{y} \\ & + \sum_{n=1}^N \int_{\partial D_n} \left(\mathbf{N}(\mathbf{x}, \mathbf{y}) \cdot \frac{\partial \mathbf{u}_m}{\partial \boldsymbol{\nu}}(\mathbf{y}) \Big|_- - \frac{\partial}{\partial \boldsymbol{\nu}_{\mathbf{y}}} \mathbf{N}(\mathbf{x}, \mathbf{y}) \cdot \mathbf{u}_m(\mathbf{y}) \Big|_- \right) d\sigma(\mathbf{y}), \quad \mathbf{x} \in \overline{\Omega}. \end{aligned}$$

By applying Green's identity (3.5) once again, but this time over $\cup_{n=1}^N D_n$, one gets

$$\begin{aligned} \mathbf{U}_m(\mathbf{x}) = & - \int_{\Omega} \mathcal{L}_{\lambda_0, \mu_0}[\mathbf{N}](\mathbf{x}, \mathbf{y}) \cdot \mathbf{u}_m(\mathbf{y}) d\mathbf{y} + \int_{\cup_{n=1}^N D_n} \mathbf{N}(\mathbf{x}, \mathbf{y}) \cdot \mathcal{L}_{\lambda_0, \mu_0}[\mathbf{u}_m](\mathbf{y}) d\mathbf{y} \\ & + \sum_{n=1}^N \int_{\partial D_n} \mathbf{N}(\mathbf{x}, \mathbf{y}) \cdot \left(\frac{\partial \mathbf{u}_m}{\partial \tilde{\nu}}(\mathbf{y}) \Big|_- - \frac{\partial \mathbf{u}_m}{\partial \nu}(\mathbf{y}) \Big|_- \right) d\sigma(\mathbf{y}), \quad \mathbf{x} \in \bar{\Omega}. \end{aligned} \quad (3.7)$$

Thanks to the first equation in (3.3) for Neumann solution \mathbf{N} , one can easily identify the first term on the RHS of (3.7) as $\mathbf{u}_m(\mathbf{x})$. Therefore, for all $\mathbf{x} \in \bar{\Omega}$

$$\begin{aligned} \mathbf{U}_m(\mathbf{x}) - \mathbf{u}_m(\mathbf{x}) = & \int_{\cup_{n=1}^N D_n} \mathbf{N}(\mathbf{x}, \mathbf{y}) \cdot \mathcal{L}_{\lambda_0, \mu_0}[\mathbf{u}_m](\mathbf{y}) d\mathbf{y} \\ & + \sum_{n=1}^N \int_{\partial D_n} \mathbf{N}(\mathbf{x}, \mathbf{y}) \cdot \left(\frac{\partial \mathbf{u}_m}{\partial \tilde{\nu}}(\mathbf{y}) \Big|_- - \frac{\partial \mathbf{u}_m}{\partial \nu}(\mathbf{y}) \Big|_- \right) d\sigma(\mathbf{y}). \end{aligned} \quad (3.8)$$

On the other hand, by using Green's identity (3.4) over $\cup_{n=1}^N D_n$, we have

$$\begin{aligned} & \int_{\cup_{n=1}^N D_n} \mathbf{N}(\mathbf{x}, \mathbf{y}) \cdot \mathcal{L}_{\lambda_0, \mu_0}[\mathbf{u}_m](\mathbf{y}) d\mathbf{y} \\ & = \sum_{n=1}^N \int_{\partial D_n} \mathbf{N}(\mathbf{x}, \mathbf{y}) \cdot \frac{\partial \mathbf{u}_m}{\partial \nu}(\mathbf{y}) \Big|_- d\sigma(\mathbf{y}) - \mathcal{Q}_{\cup_{n=1}^N D_n}^{\mathbb{C}^0}(\mathbf{N}(\mathbf{x}, \cdot), \mathbf{u}_m) \end{aligned}$$

for all $\mathbf{x} \in \bar{\Omega}$. Consequently, a few fairly easy manipulations lead us to

$$\begin{aligned} & \int_{\cup_{n=1}^N D_n} \mathbf{N}(\mathbf{x}, \mathbf{y}) \cdot \mathcal{L}_{\lambda_0, \mu_0}[\mathbf{u}_m](\mathbf{y}) d\mathbf{y} \\ & = \sum_{n=1}^N \int_{\partial D_n} \mathbf{N}(\mathbf{x}, \mathbf{y}) \cdot \left(\frac{\partial \mathbf{u}_m}{\partial \nu}(\mathbf{y}) \Big|_- - \frac{\partial \mathbf{u}_m}{\partial \tilde{\nu}}(\mathbf{y}) \Big|_- \right) d\sigma(\mathbf{y}) - \mathcal{Q}_{\cup_{n=1}^N D_n}^{\mathbb{C}^0 - \mathbb{C}}(\mathbf{N}(\mathbf{x}, \cdot), \mathbf{u}_m) \\ & \quad + \int_{\cup_{n=1}^N D_n} \mathbf{N}(\mathbf{x}, \mathbf{y}) \cdot \mathcal{L}_{\lambda, \mu}[\mathbf{u}_m](\mathbf{y}) d\mathbf{y}, \end{aligned}$$

wherein the last term vanishes thanks to second equation in (2.3). Therefore, we obtain

$$\begin{aligned} & \int_{\cup_{n=1}^N D_n} \mathbf{N}(\mathbf{x}, \mathbf{y}) \cdot \mathcal{L}_{\lambda_0, \mu_0}[\mathbf{u}_m](\mathbf{y}) d\mathbf{y} + \sum_{n=1}^N \int_{\partial D_n} \mathbf{N}(\mathbf{x}, \mathbf{y}) \cdot \left(\frac{\partial \mathbf{u}_m}{\partial \tilde{\nu}}(\mathbf{y}) \Big|_- - \frac{\partial \mathbf{u}_m}{\partial \nu}(\mathbf{y}) \Big|_- \right) d\sigma(\mathbf{y}) \\ & = - \mathcal{Q}_{\cup_{n=1}^N D_n}^{\mathbb{C}^0 - \mathbb{C}}(\mathbf{N}(\mathbf{x}, \cdot), \mathbf{u}_m), \quad \forall \mathbf{x} \in \bar{\Omega}. \end{aligned} \quad (3.9)$$

Finally, combining (3.8) and (3.9), we get

$$\mathbf{u}_m(\mathbf{x}) - \mathbf{U}_m(\mathbf{x}) = \mathcal{Q}_{\cup_{n=1}^N D_n}^{\mathbb{C}^0 - \mathbb{C}}(\mathbf{N}(\mathbf{x}, \cdot), \mathbf{u}_m), \quad \mathbf{x} \in \bar{\Omega}$$

or equivalently

$$\begin{aligned} \mathbf{u}_m(\mathbf{x}) - \mathbf{U}_m(\mathbf{x}) = & \int_{\cup_{n=1}^N D_n} \left[(\lambda_0 - \lambda(\mathbf{y})) (\nabla_{\mathbf{y}} \cdot \mathbf{N}(\mathbf{x}, \mathbf{y})) (\nabla \cdot \mathbf{u}_m(\mathbf{y})) \right. \\ & \left. + 2(\mu_0 - \mu(\mathbf{y})) \mathcal{E}[\mathbf{N}(\mathbf{x}, \cdot)](\mathbf{y}) : \mathcal{E}[\mathbf{u}_m](\mathbf{y}) \right] d\mathbf{y}, \quad \mathbf{x} \in \bar{\Omega}. \end{aligned} \quad (3.10)$$

The integral equation (3.10) provides an exact expression for the perturbations in the displacement field. However, it is precised that the Neumann function \mathbf{N} does not admit an exact explicit expression (except in a few trivial cases of simple domains such as disks and balls) in contrast to the Kelvin matrix $\mathbf{\Gamma}$ which is easily accessible. Therefore, although it is exact and valid for all $\mathbf{x} \in \bar{\Omega}$, the practical utility of the relation (3.10) is restricted. Nevertheless, a *pre-processing* of the data using Calderón preconditioner is particularly felicitous. In fact, by preconditioning integral equation (3.10) using $(-\mathcal{I}/2 + \mathcal{K}_\Omega)$ and invoking the Lemma 3.1, one can easily obtain an equivalent representation of the *filtered measurements* in terms of the Kelvin matrix as

$$\begin{aligned} \left(-\frac{1}{2}\mathcal{I} + \mathcal{K}_\Omega\right) [\mathbf{u}_m - \mathbf{U}_m](\mathbf{x}) &= \int_{\cup_{n=1}^N D_n} \left[(\lambda_0 - \lambda(\mathbf{y})) (\nabla_{\mathbf{y}} \cdot \mathbf{\Gamma}(\mathbf{x}, \mathbf{y})) (\nabla \cdot \mathbf{u}_m(\mathbf{y})) \right. \\ &\quad \left. + 2(\mu_0 - \mu(\mathbf{y})) \mathcal{E}[\mathbf{\Gamma}(\mathbf{x}, \cdot)](\mathbf{y}) : \mathcal{E}[\mathbf{u}_m](\mathbf{y}) \right] d\mathbf{y}. \end{aligned} \quad (3.11)$$

It is emphasized that, however the integral equation (3.10) is valid for all $\mathbf{x} \in \bar{\Omega}$, its preconditioned counterpart (3.11) is only valid for a.e. $\mathbf{x} \in \partial\Omega$. In order to derive an alternative integral equation valid for all $\mathbf{x} \in \Omega$, one can exploit the double layer potential \mathcal{D}_Ω in view of the jump relations (3.2) and the fact that \mathcal{D}_Ω is a solution to the elastostatic system in $\mathbb{R}^d \setminus \partial\Omega$. Precisely, for all $\mathbf{x} \in \Omega$, we have

$$\begin{aligned} \mathbf{u}_m(\mathbf{x}) - \mathbf{U}_m(\mathbf{x}) &= \mathcal{D}_\Omega [(\mathbf{u}_m - \mathbf{U}_m)|_{\partial\Omega}](\mathbf{x}) - \int_{\cup_{n=1}^N D_n} \left[(\lambda_0 - \lambda(\mathbf{y})) (\nabla_{\mathbf{y}} \cdot \mathbf{\Gamma}(\mathbf{x}, \mathbf{y})) (\nabla \cdot \mathbf{u}_m(\mathbf{y})) \right. \\ &\quad \left. + 2(\mu_0 - \mu(\mathbf{y})) \mathcal{E}[\mathbf{\Gamma}(\mathbf{x}, \cdot)](\mathbf{y}) : \mathcal{E}[\mathbf{u}_m](\mathbf{y}) \right] d\mathbf{y}. \end{aligned} \quad (3.12)$$

For completeness, the analytic expressions for different kernels involved in (3.11) and (3.12) are provided in Appendix A.

The integral equations (3.11) and (3.12) are the key components of our proposed algorithm. Different approaches based on the linearized versions or on Born and Rytov type approximations of (3.10) and (3.11) are available in the literature. In fact, the presence of \mathbf{u}_m on their right hand sides is problematic since \mathbf{u}_m is only available *a priori* on $\partial\Omega$. Unfortunately, these simplifications are not always valid and become too strong to allow an accurate reconstruction. However, as will be shown in the next section, a joint sparsity based reformulation of (3.11) in terms of unknown densities is possible if the inclusions D_1, \dots, D_N are compactly supported and *sufficiently localized* inside Ω , that is, the support set $\cup_{n=1}^N D_n$ is *sparse* in Ω . Consequently, linearization or approximations can be avoided. In the next section, we will elaborate how this allows us to recover support set $\cup_{n=1}^N D_n$ and the Lamé parameters (λ_n, μ_n) without any linearization or iterative update when multiple measurements are available.

4 Joint sparse reconstruction framework

In this section, we show that the inverse problem for spatial localization of inclusions can be recast to a joint sparse recovery problem and that the problem for quantitative evaluation of Lamé parameters becomes linear in sought parameters if the underlying inclusions are sparsely embedded in elastic formation. In particular, the integral representation (3.11) for multiple perturbed displacement fields corresponding to different applied boundary forces $\mathbf{g}_1, \dots, \mathbf{g}_M$ will be reformulated in terms of jointly sparse densities in Section 4.1. This will allow us to invoke compressed sensing algorithms for so-called *multiple measurement vector* problems

for sparse signal recovery [21, 35, 50, 54] thereby providing the unknown densities inside the support set $\cup_{n=1}^N D_n$. In Section 4.2, by using the recovered densities together with (3.12), we will show that it is possible to accurately estimate the displacement and strain inside the inclusions and consequently the inverse problem for parameter reconstruction becomes linear. The discretization of these formulations will be discussed in Section 4.3.

4.1 Integral formulation using jointly sparse densities and support identification

Let us first investigate the integral formulation (3.11) subject to multiple boundary forces. Towards this end, let $\mathbf{A}^i : \mathbb{R}^d \times \mathbb{R}^d \rightarrow \mathbb{R}^{1 \times 1}$, $\mathbf{B}^i : \mathbb{R}^d \times \mathbb{R}^d \rightarrow \mathbb{R}^{d \times d}$, $\mathbf{X}_m^1 : \mathbb{R}^d \rightarrow \mathbb{R}^{1 \times 1}$, and $\mathbf{X}_m^2 : \mathbb{R}^d \rightarrow \mathbb{R}^{d \times d}$, for all $i = 1, \dots, d$ and $m = 1, \dots, M$, be defined by

$$\begin{aligned} \mathbf{A}^i(\mathbf{x}, \mathbf{y}) &:= \left([\nabla \cdot \boldsymbol{\Gamma}(\mathbf{x}, \mathbf{y})]_i \right), \quad \mathbf{B}^i(\mathbf{x}, \mathbf{y}) := \text{slice}_1 \left(i, \mathcal{E}[\boldsymbol{\Gamma}](\mathbf{x}, \mathbf{y}) \right), \quad \mathbf{x} \neq \mathbf{y}, \\ \mathbf{X}_m^1(\mathbf{y}) &:= [\lambda_0 - \lambda(\mathbf{y})] \left(\nabla \cdot \mathbf{u}_m(\mathbf{y}) \right), \quad \mathbf{X}_m^2(\mathbf{y}) := 2 [\mu_0 - \mu(\mathbf{y})] \mathcal{E}[\mathbf{u}_m](\mathbf{y}). \end{aligned}$$

With these definitions at hand, (3.11) can be rewritten as

$$\begin{aligned} \left(-\frac{1}{2}\mathcal{I} + \mathcal{K}_\Omega \right) [\mathbf{u}_m - \mathbf{U}_m](\mathbf{x}) &= \int_{\cup_{n=1}^N D_n} \sum_{i=1}^d \left[\mathbf{A}^i(\mathbf{x}, \mathbf{y}) : \mathbf{X}_m^1(\mathbf{y}) + \mathbf{B}^i(\mathbf{x}, \mathbf{y}) : \mathbf{X}_m^2(\mathbf{y}) \right] \hat{\mathbf{e}}_i d\mathbf{y} \\ &= \int_{\cup_{n=1}^N D_n} \sum_{i=1}^d \left[\text{vec}(\mathbf{A}^i(\mathbf{x}, \mathbf{y}))^\top \text{vec}(\mathbf{X}_m^1(\mathbf{y})) + \text{vec}(\mathbf{B}^i(\mathbf{x}, \mathbf{y}))^\top \text{vec}(\mathbf{X}_m^2(\mathbf{y})) \right] \hat{\mathbf{e}}_i d\mathbf{y} \quad (4.1) \end{aligned}$$

for all $\mathbf{x} \in \partial\Omega$. Now we introduce $\mathbf{X}_m : \cup_{n=1}^N D \rightarrow \mathbb{R}^{d^2+1}$, $\boldsymbol{\Lambda} : \cup_{n=1}^N D \times \cup_{n=1}^N D \rightarrow \mathbb{R}^{d \times (d^2+1)}$ and $\mathbf{Y}_m : \partial\Omega \rightarrow \mathbb{R}^d$ by

$$\mathbf{X}_m(\mathbf{y}) := \begin{pmatrix} \text{vec}(\mathbf{X}_m^1(\mathbf{y})) \\ \text{vec}(\mathbf{X}_m^2(\mathbf{y})) \end{pmatrix}, \quad \boldsymbol{\Lambda}(\mathbf{x}, \mathbf{y}) := \begin{pmatrix} \text{vec}(\mathbf{A}^1(\mathbf{x}, \mathbf{y}))^\top & \text{vec}(\mathbf{B}^1(\mathbf{x}, \mathbf{y}))^\top \\ \vdots & \vdots \\ \text{vec}(\mathbf{A}^d(\mathbf{x}, \mathbf{y}))^\top & \text{vec}(\mathbf{B}^d(\mathbf{x}, \mathbf{y}))^\top \end{pmatrix}$$

and

$$\mathbf{Y}_m(\mathbf{x}) := \left(-\frac{1}{2}\mathcal{I} + \mathcal{K}_\Omega \right) [\mathbf{u}_m - \mathbf{U}_m](\mathbf{x})$$

so that, from (4.1), we have

$$\mathbf{Y}_m(\mathbf{x}) = \int_{\cup_{n=1}^N D_n} \boldsymbol{\Lambda}(\mathbf{x}, \mathbf{y}) \mathbf{X}_m(\mathbf{y}) d\mathbf{y}, \quad \mathbf{x} \in \partial\Omega. \quad (4.2)$$

Remark that the integral in (4.2) has to be evaluated over the unknown support of inclusions. In order to furnish an integral equation that does not require *a priori* information of the unknown support of inclusions, we simply extend the function \mathbf{X}_m by zero outside $\cup_{n=1}^N D_n$, that is, we consider its extension

$$\tilde{\mathbf{X}}_m := \begin{cases} \mathbf{X}_m(\mathbf{y}) & \text{for } \mathbf{y} \in \cup_{n=1}^N D_n \\ \mathbf{0} & \text{for } \mathbf{y} \in \Omega \setminus \cup_{n=1}^N \overline{D_n} \end{cases}$$

so that

$$\mathbf{Y}_m(\mathbf{x}) = \int_{\Omega} \mathbf{\Lambda}(\mathbf{x}, \mathbf{y}) \tilde{\mathbf{X}}_m(\mathbf{y}) d\mathbf{y}, \quad \mathbf{x} \in \partial\Omega. \quad (4.3)$$

It is very interesting to note that the inclusions are compactly embedded well inside the background domain Ω thanks to assumption H1 and are located at fixed positions despite of the different applied boundary forces $\mathbf{g}_1, \dots, \mathbf{g}_M$. Moreover, the density $\tilde{\mathbf{X}}_m$ varies only at the support of the inclusions D_1, \dots, D_N for each excitation but is zero elsewhere independent of the measurement data \mathbf{Y}_m . Therefore, assuming sparsity for the support set $\cup_{n=1}^N D_N$ in Ω , the problem of inclusion detection from (4.3) can be regarded as a joint sparse recovery problem of $\tilde{\mathbf{X}}_m(\mathbf{y}), m = 1, \dots, M$, which has been extensively investigated in compressed sensing literature [18, 35]. A detailed implementation including the discretization of (4.3) for joint sparse recovery will be discussed later. Once the density $\tilde{\mathbf{X}}_m(\mathbf{y}), m = 1, \dots, M$, is reconstructed using a joint sparse recovery algorithm, the support of the inclusions can be easily identified by investigating the magnitude of $\tilde{\mathbf{X}}_m(\mathbf{y}), m = 1, \dots, M$.

4.2 Recovery of constitutive parameters

In the sequel, the notation \hat{D} is adopted for the entire reconstructed support $\cup_{n=1}^N D_n$ by virtue of joint sparse recovery step. Similarly, $\hat{\mathbf{X}}_m(\mathbf{y})$ (and, accordingly, $\hat{\mathbf{X}}_m^1(\mathbf{y}), \hat{\mathbf{X}}_m^2(\mathbf{y})$) will denote the estimated densities. The second step of the proposed algorithm dealing with the parameter evaluation is based on the integral equation (3.12). Precisely, we first estimate the total displacement field for all $\mathbf{x} \in \hat{D}$ using the recursive relationship

$$\begin{aligned} \hat{\mathbf{u}}_m(\mathbf{x}) &= \mathbf{U}_m(\mathbf{x}) + \mathcal{D}_{\Omega} [(\mathbf{u}_m - \mathbf{U}_m)|_{\partial\Omega}] (\mathbf{x}) \\ &\quad - \int_{\hat{D}} \sum_{i=1}^d \left[\mathbf{A}^i(\mathbf{x}, \mathbf{y}) : \hat{\mathbf{X}}_m^1(\mathbf{y}) + \mathbf{B}^i(\mathbf{x}, \mathbf{y}) : \hat{\mathbf{X}}_m^2(\mathbf{y}) \right] \hat{\mathbf{e}}_i d\mathbf{y}, \end{aligned}$$

where $\hat{\mathbf{u}}_m$ is the calculated total field over \hat{D} at this step and all the terms on the RHS are obtained either from the measurements or the first step. Consequently, quantities $\nabla \cdot \hat{\mathbf{u}}_m$ and $\mathcal{E}(\hat{\mathbf{u}}_m)$ can also be computed from $\hat{\mathbf{u}}_m$ for all $\mathbf{x} \in \hat{D}$. Finally, we can once again invoke the integral formulation (3.11) or equivalently its matrix form (4.2) to formulate another problem with slightly modified sensing matrix and new unknowns $(\lambda_0 - \lambda)$ and $(\mu_0 - \mu)$. Indeed, from (4.2), we have

$$\mathbf{Y}_m(\mathbf{x}) = \int_{\hat{D}} \mathbf{\Lambda}(\mathbf{x}, \mathbf{y}) \hat{\mathbf{X}}_m(\mathbf{y}) d\mathbf{y} = \int_{\hat{D}} \tilde{\mathbf{\Lambda}}_m(\mathbf{x}, \mathbf{y}) \mathbf{Z}(\mathbf{y}) d\mathbf{y}, \quad (4.4)$$

where $\tilde{\mathbf{\Lambda}}_m : \cup_{n=1}^N D_n \times \cup_{n=1}^N D_n \rightarrow \mathbb{R}^{d \times (d^2+1)}$ and $\mathbf{Z} : \cup_{n=1}^N D_n \rightarrow \mathbb{R}^{d^2+1}$ are defined by

$$\begin{aligned} \tilde{\mathbf{\Lambda}}_m(\mathbf{x}, \mathbf{y}) &:= \mathbf{\Lambda}(\mathbf{x}, \mathbf{y}) \text{diag} \left(\nabla \cdot \hat{\mathbf{u}}_m(\mathbf{y}), \text{vec}(2\mathcal{E}(\hat{\mathbf{u}}_m)(\mathbf{y}))^\top \right), \\ \mathbf{Z}(\mathbf{y}) &:= (\lambda_0 - \lambda(\mathbf{y}), \quad \mu_0 - \mu(\mathbf{y}), \quad \dots, \quad \mu_0 - \mu(\mathbf{y}))^\top. \end{aligned}$$

We emphasize that the problem (4.4) is *linear* for \mathbf{Z} since the support set \hat{D} and the modified sensing matrix $\tilde{\mathbf{\Lambda}}_m$ on it are completely known. Thus, no linearization or iterative update is required to solve (4.4). Moreover, the second step of inverse problem is expected to be efficient and less ill-posed due to the knowledge of the estimated position of anomalies.

4.3 Discretization of the integral formulations

In this section, we will investigate how the findings of the Sections 4.1 and 4.2 can be realized in a discrete setting.

4.3.1 First step: Discretization of (4.3)

For numerical implementation, let us assume that $\tilde{\mathbf{X}}_m$ is approximated by either piece wise constant functions or splines as

$$\left[\tilde{\mathbf{X}}_m(\mathbf{y})\right]_q = \sum_{\ell=1}^L \left[\tilde{\mathbf{X}}_m(\mathbf{y}_\ell)\right]_q \varphi_q(\mathbf{y}, \mathbf{y}_\ell), \quad \forall q \in \{1, \dots, d^2 + 1\}, \mathbf{y} \in \Omega,$$

where $\{\mathbf{y}_\ell\}_{\ell=1}^L$, for some $L \in \mathbb{N}$, are the finite sampling points of Ω and $\varphi_q(\mathbf{y}, \mathbf{y}_\ell)$ is the basis function for the q -th coordinate with $q \in \{1, \dots, d^2 + 1\}$.

Using measurement points $\{\mathbf{x}_r\}_{r=1}^R \subset \partial\Omega$ and sampling points $\{\mathbf{y}_\ell\}_{\ell=1}^L \in \Omega$ we introduce the unknown density $\mathfrak{X} \in \mathbb{R}^{(d^2+1)L \times M}$, the measurement matrix $\mathfrak{Y} \in \mathbb{R}^{dR \times M}$ and the sensing matrix $\mathbf{\Pi} \in \mathbb{R}^{dR \times (d^2+1)L}$ by

$$\mathfrak{X} := \begin{pmatrix} \mathfrak{X}_1 \\ \vdots \\ \mathfrak{X}_{d^2+1} \end{pmatrix}, \quad \mathfrak{Y} := \begin{pmatrix} \mathfrak{Y}_1 \\ \vdots \\ \mathfrak{Y}_d \end{pmatrix} \quad \text{and} \quad \mathbf{\Pi} := \begin{pmatrix} \mathbf{\Pi}_{11} & \cdots & \mathbf{\Pi}_{1(d^2+1)} \\ \vdots & \ddots & \vdots \\ \mathbf{\Pi}_{d1} & \cdots & \mathbf{\Pi}_{d(d^2+1)} \end{pmatrix},$$

where the element matrices $\mathfrak{X}_q \in \mathbb{R}^{L \times M}$, $\mathfrak{Y}_p \in \mathbb{R}^{R \times M}$ and $\mathbf{\Pi}_{pq} \in \mathbb{R}^{R \times L}$ are defined by

$$[\mathfrak{X}_q]_{\ell m} := \left[\tilde{\mathbf{X}}_m(\mathbf{y}_\ell)\right]_q, \quad [\mathfrak{Y}_p]_{rm} := [\mathbf{Y}_m(\mathbf{x}_r)]_p, \quad [\mathbf{\Pi}_{pq}]_{r\ell} := \int_{\Omega} [\mathbf{\Lambda}(\mathbf{x}_r, \mathbf{z})]_{pq} \varphi_q(\mathbf{z}, \mathbf{y}_\ell) d\mathbf{z},$$

for all $p \in \{1, \dots, d\}$, $q \in \{1, \dots, d^2 + 1\}$, $r \in \{1, \dots, R\}$ and $\ell \in \{1, \dots, L\}$. The aforementioned discretization and definitions then render the system of linear equations

$$\mathfrak{Y} = \mathbf{\Pi} \mathfrak{X}. \quad (4.5)$$

The following remarks are in order. First, there are usually more sampling points $\mathbf{y}_\ell \in \Omega$ than the measurement points $\mathbf{x}_r \in \partial\Omega$ in practice. Therefore, the linear system (4.5) is practically very under-determined, that is, $dR \ll (d^2 + 1)L$. Therefore, there is no uniqueness of the solution without assuming any prior knowledge. Second, the unknown density matrix \mathfrak{X} is sparse thanks to its construction and the assumption of the sparsity of the support set $\cup_{n=1}^N D_n$ in Ω . In fact, in the aforementioned discrete setup the non-zero rows of \mathfrak{X} are those that correspond to the locations $\mathbf{y}_\ell \in \cup_{n=1}^N D_n$. These two observations naturally lead us to exploit the joint sparsity as a prior information. As will be discussed at a later stage, there are several joint sparse recovery algorithms to uniquely solve system (4.5). Therefore, by solving the linear system using any one of those algorithms, the unknown density \mathfrak{X} can be recovered which in turn gives access to the support of the inclusions and the perturbed displacement field inside the support of the inclusions.

4.3.2 Second step: Discretization of (4.4)

The formulation (4.4) renders another under-determined system of linear equations in the discrete setting and $\mathbf{Z}(\mathbf{y}_\ell)$ for all $\mathbf{y}_\ell \in \hat{D}$ can be obtained by solving another constraint optimization

problem. Towards this end, let $\{\hat{\mathbf{y}}_\ell\}_{\ell=1}^{\tilde{L}}$ be the collection of sampling points that belong to the support set \hat{D} with $\tilde{L} \ll L$. Then, by fairly easy manipulations similar to those in Section 4.3.1, the descretized version of (4.4) is obtained as

$$\tilde{\mathbf{Y}} = \tilde{\mathbf{\Pi}} \tilde{\mathbf{Z}} \quad (4.6)$$

with

$$\tilde{\mathbf{Y}} := \begin{pmatrix} \tilde{\mathbf{Y}}_1 \\ \tilde{\mathbf{Y}}_2 \\ \vdots \\ \tilde{\mathbf{Y}}_M \end{pmatrix} \in \mathbb{R}^{MdR}, \quad \tilde{\mathbf{Z}} := \begin{pmatrix} \tilde{\mathbf{Z}}_1 \\ \tilde{\mathbf{Z}}_2 \\ \vdots \\ \tilde{\mathbf{Z}}_{d^2+1} \end{pmatrix} \in \mathbb{R}^{(d^2+1)\tilde{L}}, \quad \tilde{\mathbf{\Pi}} := \begin{pmatrix} \tilde{\mathbf{\Pi}}_1 \\ \tilde{\mathbf{\Pi}}_2 \\ \vdots \\ \tilde{\mathbf{\Pi}}_M \end{pmatrix} \in \mathbb{R}^{MdR \times (d^2+1)\tilde{L}},$$

where

$$\tilde{\mathbf{\Pi}}_m = \begin{pmatrix} \tilde{\mathbf{\Pi}}_{m11} & \cdots & \tilde{\mathbf{\Pi}}_{m1(d^2+1)} \\ \vdots & \ddots & \vdots \\ \tilde{\mathbf{\Pi}}_{md1} & \cdots & \tilde{\mathbf{\Pi}}_{md(d^2+1)} \end{pmatrix} \quad \text{with} \quad [\tilde{\mathbf{\Pi}}_{mpq}]_{r\ell} = \int_{\hat{D}} [\tilde{\mathbf{\Lambda}}_m(\mathbf{x}_r, \mathbf{y})]_{pq} \varphi_q(\mathbf{y}, \hat{\mathbf{y}}_\ell) d\mathbf{y},$$

$$\tilde{\mathbf{Z}}_q = \begin{pmatrix} [\mathbf{Z}(\hat{\mathbf{y}}_1)]_q \\ \vdots \\ [\mathbf{Z}(\hat{\mathbf{y}}_{\tilde{L}})]_q \end{pmatrix} \quad \text{and} \quad \tilde{\mathbf{Y}}_m = \begin{pmatrix} \tilde{\mathbf{Y}}_{m1} \\ \vdots \\ \tilde{\mathbf{Y}}_{md} \end{pmatrix} \quad \text{with} \quad \tilde{\mathbf{Y}}_{mp} = \begin{pmatrix} [\mathbf{Y}_m(\mathbf{x}_1)]_p \\ \vdots \\ [\mathbf{Y}_m(\mathbf{x}_R)]_p \end{pmatrix}$$

for all $p \in \{1, \dots, d\}$, $q \in \{1, \dots, d^2 + 1\}$, $m \in \{1, \dots, M\}$, $\ell \in \{1, \dots, \tilde{L}\}$ and $r \in \{1, \dots, R\}$. Note that the number of unknowns in the discretized domain is reduced from $(d^2 + 1)L$ to $(d^2 + 1)\tilde{L}$, whereas the sensing matrix $\tilde{\mathbf{\Pi}}$ is accurate if the estimates of $\hat{\mathbf{y}}_\ell$ and $\hat{\mathbf{u}}_m$ are precise.

5 Implementation of the proposed algorithm

Let us now provide detailed implementation of the proposed reconstruction algorithm. In particular, we will investigate how the two discrete inverse problems (4.5) and (4.6) can be addressed. Note that problem (4.5) has a prior constraint that the number of non-zero rows is sparse, whereas problem (4.6) is a classical linear ill-posed problem. Therefore, the two problems should be addressed separately. In the following, the compressed sensing approach for joint sparse recovery will be reviewed in Section 5.1, and then a modified version of Multiple Sparse Bayesian Learning (M-SBL) algorithm will be explained in Section 5.2 as our joint sparse recovery algorithm to solve (4.5). For the second step, we will discuss the details of the Constrained Split Augmented Lagrangian Shrinkage Algorithm (C-SALSA) implementation to solve (4.6) in Section 5.3.

5.1 Compressed sensing for joint sparse recovery problems

Compressed Sensing (CS) theory is the state of the art in the field of signal processing that enables the recovery of the signals beyond the Nyquist limit based on their sparsity [16]. As an example, let us consider the under-determined linear system $\mathbf{y} = \mathbf{\Pi} \mathbf{x}$ that has many solutions.

One of the most important innovations of CS is that when the signal \mathbf{x} is sparse, its accurate recovery is possible using the sparse recovery problem

$$\min_{\mathbf{x}} \|\mathbf{x}\|_0 \quad \text{subject to } \mathbf{y} = \mathbf{\Pi}\mathbf{x}, \quad (5.1)$$

where $\mathbf{y} \in \mathbb{R}^J$, $\mathbf{\Pi} \in \mathbb{R}^{J \times K}$, and $\mathbf{x} \in \mathbb{R}^K$ with $J < K$ (see, for instance, [16]). Here $\|\mathbf{x}\|_0$ denotes the number of non-zero elements in the vector \mathbf{x} . The uniqueness of the solution to the problem (5.1) is guaranteed by the condition

$$\|\mathbf{x}\|_0 < \frac{\text{spark}(\mathbf{\Pi})}{2},$$

where $\text{spark}(\mathbf{\Pi})$ is the smallest possible number ℓ such that there exist ℓ linearly dependent columns of $\mathbf{\Pi}$ [24]. Since (5.1) is an *NP-hard* problem, a convex relaxation using l_1 -minimization widely used in practice is

$$\min_{\mathbf{x}} \|\mathbf{x}\|_1 \quad \text{subject to } \mathbf{y} = \mathbf{\Pi}\mathbf{x}, \quad (5.2)$$

where $\|\cdot\|_1$ denotes the l_1 -norm. The beauty of compressed sensing is that (5.2) provides exactly the same solution as (5.1) if the so called *restricted isometry property* (RIP) is satisfied [17]. It has been shown that for many classes of random matrices, the RIP is satisfied with extremely high probability if the number of measurement satisfies $J \geq c\|\mathbf{x}\|_0 \log(K/\|\mathbf{x}\|_0)$, where c is an absolute constant [17].

The Multiple Measurement Vector (MMV) problem is a generalization of the Single Measurement Vector (SMV) problem defined in (5.1) [18, 35]. It is the signal recovery problem to exploit a set of sparse signal vectors that share common non-zero supports, that is, a set of signal vectors that have *joint sparsity*. Specifically, let $\|\mathfrak{X}\|_0$ denote the number of rows that have non-zero elements in the matrix \mathfrak{X} . Then, the MMV problem addresses the following:

$$\min_{\mathfrak{X}} \|\mathfrak{X}\|_0 \quad \text{subject to } \mathfrak{Y} = \mathbf{\Pi}\mathfrak{X}, \quad (5.3)$$

where $\mathfrak{Y} \in \mathbb{R}^{J \times M}$, $\mathfrak{X} \in \mathbb{R}^{K \times M}$, and M denotes the number of measurement vectors. Since the MMV problem (5.3) contains more information than the SMV problem (5.1) (except in the degenerate case when all columns of \mathfrak{Y} are linearly dependent), it provides better reconstruction results. Theoretically, problem (5.3) has unique solution if and only if

$$\|\mathfrak{X}\|_0 < \frac{\text{spark}(\mathfrak{A}) + \text{rank}(\mathfrak{Y}) - 1}{2}, \quad (5.4)$$

where $\text{rank}(\mathfrak{Y})$ denotes the rank of \mathfrak{Y} which may increase with the number of measurement vectors [18, 23]. Note that (5.4) is just an algebraic bound for the noiseless measurements. In practice, the number of measurements can be reduced proportional to the number of multiple measurement vectors, i.e. $J \geq (c/M)\|\mathfrak{X}\|_0 \log(K/\|\mathfrak{X}\|_0)$ [35].

There are various types of joint sparse recovery algorithms to solve the MMV problem including the convex relaxation [21, 35, 50, 54]. Among those, we choose the M-SBL algorithm [54] due to its robustness for noise. The detailed description of M-SBL with its specific modification to the problem under investigation is provided in the next section.

5.2 M-SBL implementation

It is worthwhile precising that M-SBL algorithm was initially derived based on the assumption that the noise and the unknown signal follow an independent and identically distributed (i.i.d)

zero mean Gaussian distributions. However, recent theoretical analysis substantiates that M-SBL is in fact a sparse recovery algorithm that can be used in deterministic framework without assuming any statistics for the unknown signal (see, for instance, [55]). More specifically, it solves the minimization problem

$$\min_{\mathfrak{X}} \|\mathfrak{Y} - \mathbf{\Pi}\mathfrak{X}\|_F^2 + \zeta \mathcal{R}_\zeta(\mathfrak{X}), \quad (5.5)$$

wherein the penalty function $\mathcal{R}_\zeta(\mathfrak{X})$ is given by

$$\mathcal{R}_\zeta(\mathfrak{X}) := \min_{g_i \geq 0, \forall i=1, \dots, (d^2+1)L} \text{tr}(\mathfrak{X}^* \mathbf{G}^{-1} \mathfrak{X}) + M \log |\det(\mathbf{\Pi} \mathbf{G} \mathbf{\Pi}^* + \zeta \mathbf{I}_{dR})|,$$

with tr indicating the trace of a matrix and the superposed $*$ reflecting a Hermitian conjugate, that is, $\mathbf{A}^* = \overline{\mathbf{A}}^\top$. Here ζ is a regularization hyper-parameter controlling the relative weights of the two terms and provides a trade-off between fidelity to the measurements and noise sensitivity, and $\mathbf{G} \in \mathbb{R}^{(d^2+1)L \times (d^2+1)L}$ is a diagonal matrix with entries $[\mathbf{G}]_{ii} := g_i$ indicating the sparseness of the respective rows of \mathfrak{X} . We emphasize that, thanks to its non-separating nature, the M-SBL penalty function \mathcal{R}_ζ imposes the sparsity more effectively than the conventional l^p -norms. We refer the interested readers to [55] for a detailed topical discussion.

It is interesting to note that by construction the unknown matrix \mathfrak{X} has a special block structure for elasticity imaging unlike the general joint sparse signal recovery problems. In fact, the density \mathfrak{X} is a block matrix composed of $(d^2 + 1)$ sub-matrices vertically stacked and each one of those has exactly same joint sparsity structure. The sparsity structure of elastostatic problem for $d = 2$ is delineated in Figure 1. Moreover, since it is really inevitable to avoid measurement noise in practice, it is more appropriate to consider the noisy linear system

$$\mathfrak{Y} = \mathbf{\Pi}\mathfrak{X} + \mathbf{E} \quad (5.6)$$

than the system (4.5). Here $\mathbf{E} \in \mathbb{R}^{dR \times M}$ represents additive measurement noise. Therefore, the joint sparse recovery problem corresponding to (5.6) subject to the aforementioned structural constraint is given by

$$\min_{\mathfrak{X} \in \mathcal{M}_{\text{ad}}} \|\mathfrak{X}\|_0 \quad \text{subject to } \|\mathfrak{Y} - \mathbf{\Pi}\mathfrak{X}\|_F \leq \epsilon, \quad (5.7)$$

where $\mathcal{M}_{\text{ad}} \subset \mathbb{R}^{(d^2+1)L \times M}$ is the set of admissible matrices that have aforementioned block structure and $\epsilon > 0$ is a noise dependent parameter.

5.2.1 Signal recovery

In order to solve the joint sparsity problem (5.7), we propose a modified version of M-SBL algorithm with structural constraint. Precisely, the general optimization problem (5.5) is modified as

$$\min_{\mathfrak{X}} \|\mathfrak{Y} - \mathbf{\Pi}\mathfrak{X}\|_F^2 + \zeta \mathcal{R}_\zeta(\mathfrak{X}) + \mathbb{1}_{\mathcal{M}_{\text{ad}}}(\mathfrak{X}),$$

where $\mathbb{1}_{\mathcal{M}_{\text{ad}}}$ denotes the indicator function of \mathcal{M}_{ad} , that is,

$$\mathbb{1}_{\mathcal{M}_{\text{ad}}}(\mathbf{w}) := \begin{cases} 0, & \mathbf{w} \in \mathcal{M}_{\text{ad}}, \\ \infty, & \text{otherwise.} \end{cases}$$

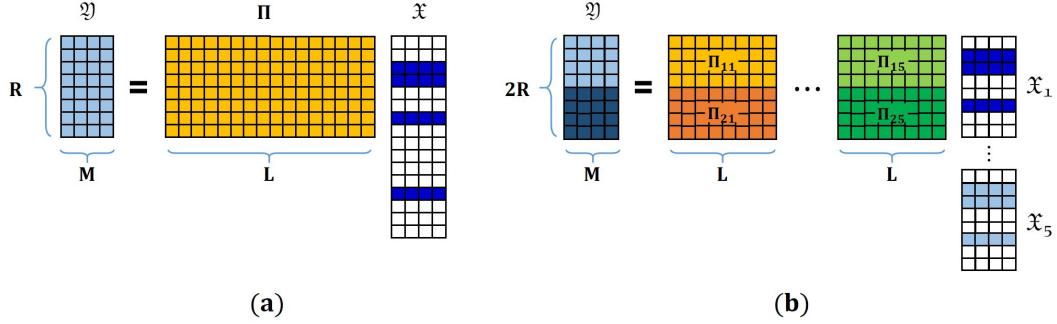


Figure 1: Joint sparsity models in 2D. (a) General problem. (b) Elastostatic problem.

Owing to the structural constraint on unknown density \mathfrak{X} , the associated structured sparsities are updated simultaneously using the constraint

$$g_\ell = g_{\ell+L} = \dots = g_{\ell+d^2L}, \quad \forall \ell = 1, \dots, L.$$

The step-by-step procedure for the modified M-SBL is summarized in Algorithm 1.

Algorithm 1 Modified M-SBL for sparse signal recovery in elasticity imaging.

- 1: Set iterations $\text{Iter}_{\max} \geq 1$ and threshold $1 \gg \varrho > 0$.
- 2: Set σ_{\max} to be the largest singular value of Π .
- 3: Set $k := 0$ and $\zeta^{(0)} := 10 \times \sigma_{\max}^2$.
- 4: Set $g_\ell^{(0)} := 1$ for $\ell = 1, 2, \dots, (d^2 + 1)L$ and $\mathbf{G}^{(0)} := \text{diag}(g_1^{(0)}, g_2^{(0)}, \dots, g_{(d^2+1)L}^{(0)})$.
- 5: Set $\pi_\ell := ([\Pi]_{1\ell}, \dots, [\Pi]_{(dR)\ell})^\top$ and $\pi_\ell^* := ([\Pi]_{1\ell}^*, \dots, [\Pi]_{(dR)\ell}^*)^\top$.
- 6: **for** $k = 1, \dots, \text{Iter}_{\max}$ **do**
- 7: Set $\mathbf{F}^{(k-1)} := (\Pi \mathbf{G}^{(k-1)} \Pi^* + \zeta^{(k-1)} \mathbf{I}_{dR})^{-1}$.
- 8: Update $\mathfrak{X}^{(k)} = \mathbf{G}^{(k-1)} \Pi^* \mathbf{F}^{(k-1)} \mathfrak{Y}$.
- 9: Update: for $\ell = 1, \dots, L$

$$g_\ell^{(k)} = g_{\ell+L}^{(k)} = \dots = g_{\ell+d^2L}^{(k)} = \sqrt{\sum_{q=1}^{d^2+1} \sum_{m=1}^M \left| [\mathfrak{X}_q^{(k)}]_{\ell m} \right|^2 / M \sum_{p=0}^{d^2L} \pi_{\ell+p}^* \mathbf{F}^{(k-1)} \pi_{\ell+p}}.$$

- 10: Set $\mathbf{G}^{(k)} := \text{diag}(g_1^{(k)}, g_2^{(k)}, \dots, g_{(d^2+1)L}^{(k)})$.
 - 11: **if** $g_\ell^{(k)} / \max_\ell (g_\ell^{(k)}) < \varrho$ **then**
 - 12: $g_\ell^{(k)} = 0$
 - 13: **end if**
 - 14: Update $\zeta^{(k)} = \sqrt{\|\mathfrak{Y} - \Pi \mathfrak{X}^{(k)}\|_F^2 / M \text{tr}(\mathbf{F}^{(k-1)})}$.
 - 15: **end for** **return** $\hat{\mathfrak{X}} := \mathfrak{X}^{(k)}$
-

5.2.2 Preconditioning

We recall that the problem (5.6) is severely ill-posed if the inclusions are extended and not really sparse inside the background domain due to the intrinsic ill-posedness of the elasticity imaging problem. Moreover, the sensing matrix, which is associated to a physical system, has a coherence structure and its columns are not completely incoherent. This affects the performance of the sparsity based recovery algorithms. Therefore, it is desirable to introduce a surgical preconditioning procedure before executing M-SBL algorithm. Towards this end, we consider the singular value decomposition of the sensing matrix as $\mathbf{\Pi} = \mathbf{V}\mathbf{\Sigma}\mathbf{W}^*$ where $\mathbf{\Sigma} \in \mathbb{R}^{dR \times (d^2+1)L}$ is such that $[\mathbf{\Sigma}]_{rr} =: \sigma_r$, for all $r = 1, \dots, dR$, are the singular values of $\mathbf{\Pi}$ and $[\mathbf{\Sigma}]_{r\ell} = 0$ for all $r \neq \ell$. The matrices $\mathbf{V} \in \mathbb{R}^{dR \times dR}$ and $\mathbf{W} \in \mathbb{R}^{(d^2+1)L \times (d^2+1)L}$ are unitary and their columns are respectively the left and right singular vectors of $\mathbf{\Pi}$. Consequently, a preconditioning weight matrix $\mathbf{P} \in \mathbb{R}^{dR \times dR}$ can be introduced as

$$\mathbf{P} = (\mathbf{\Sigma}^2 + \theta \mathbf{I}_{dR})^{-1/2} \mathbf{V}^*$$

with θ being a thresholding parameter (refer, for instance, to [34, 38]). The M-SBL algorithm can then be applied to the regularized problem

$$\mathbf{P}\mathfrak{Y} = \mathbf{P}\mathbf{\Pi}\mathfrak{X} + \mathbf{P}\mathbf{E}. \quad (5.8)$$

5.2.3 Support identification

The application of M-SBL Algorithm 1 renders the unique minimizer $\hat{\mathfrak{X}}$ to the constraint optimization problem (5.7). Having recovered the sparse signal vector, we now identify the support set $\cup_{n=1}^N D_n$ by collecting all \mathbf{y}_ℓ such that $[\tilde{\mathbf{X}}_m(\mathbf{y}_\ell)]_q$ is nonzero for all $q = 1, \dots, d^2 + 1$ and $m = 1, \dots, M$. In other words, we look for $\ell \in \{1, \dots, L\}$ such that $[\hat{\mathfrak{X}}_q]_{\ell m}$ is non-zero for all $q = 1, \dots, d^2 + 1$ and $m = 1, \dots, M$. Towards this end, we set

$$\hat{D} := \left\{ \mathbf{y}_\ell \mid \psi_\ell / \max_{\ell \in \{1, \dots, L\}} (\psi_\ell) > \xi \right\}, \quad (5.9)$$

where ξ is a pruning parameter and ψ_ℓ is defined by

$$\psi_\ell := \sqrt{\sum_{q=1}^{d^2+1} \sum_{m=1}^M \left| [\hat{\mathfrak{X}}_q]_{\ell m} \right|^2}, \quad 1 \leq \ell \leq L.$$

Note that ψ_ℓ indicates the sparseness of the ℓ -th row. Because of the numerical implementation, the values of $[\hat{\mathfrak{X}}_q]_{\ell m}$ cannot reach zero absolutely, though they may be very small. Therefore, this pruning step is indispensable to sweep away the values smaller than a predefined threshold depending on the noise level and numerical discretization.

5.3 Parameter reconstruction

For the quantitative evaluation of the of Lamé parameters of \hat{D} , we need to solve system (4.6). Towards this end, we formulate the constrained optimization problem

$$\arg \min_{\mathfrak{Z}} \|\mathfrak{Z}\|_1 \quad \text{subject to } \|\tilde{\mathbf{Y}} - \tilde{\mathbf{\Pi}}\mathfrak{Z}\|_2 \leq \eta, \quad \theta_{\min} \leq [\mathfrak{Z}]_i \leq \theta_{\max}, \quad i = 1, \dots, (d^2 + 1)\tilde{L}, \quad (5.10)$$

where l_1 –penalty is enforced in order to achieve noise robust reconstruction and the constraint

$$\theta_{\min} \leq [\mathbf{3}]_i \leq \theta_{\max} \quad (5.11)$$

emerges from the assumption H3. Here θ_{\min} and θ_{\max} are real numbers such that $\theta_{\min} \leq \theta_{\max}$ and ζ is the constraint weight.

There are several algorithms available in the literature that are tailored to solve such constrained optimization problems and any one of them can be deployed to resolve (5.10). We present in this section the procedure and detailed implementation of the C-SALSA by Afonso, Bioucas-Dias, and Figueiredo [1] in order to recover Lamé parameters of \hat{D} . An adaptive pseudo-code implementation of C-SALSA is furnished in Algorithm 2. Beforehand, we normalize the sensing matrix $\tilde{\mathbf{\Pi}}$ so that each one of its columns has a unit l_2 –norm, whereas we continue denoting it with $\tilde{\mathbf{\Pi}}$ after normalization by abuse of notation. The idea of C-SALSA is to first transform the constrained optimization problem into an unconstrained problem which in turn is further transformed using a variable splitting operation before finally being resolved using *Alternating Direction Method of Multipliers* (ADMM). The interested readers are referred to [1] for a topical review and detailed account of C-SALSA.

Let $\mathcal{B}_\eta(\tilde{\mathbf{Y}})$ be the Euclidean ball in \mathbb{R}^{MdR} centered at $\tilde{\mathbf{Y}}$ and radius η . Then the problem (5.10) can be equivalently written as the unconstrained problem (see [1])

$$\min_{\mathbf{3}} \tilde{\zeta} \|\mathbf{3}\|_1 + \mathbb{1}_{\mathcal{B}_\eta(\tilde{\mathbf{Y}})}(\tilde{\mathbf{\Pi}}\mathbf{3}), \quad (5.12)$$

where $\mathbb{1}_{\mathcal{B}_\eta(\tilde{\mathbf{Y}})}$ is the indicator function of $\mathcal{B}_\eta(\tilde{\mathbf{Y}})$, that is,

$$\mathbb{1}_{\mathcal{B}_\eta(\tilde{\mathbf{Y}})}(\mathbf{w}) := \begin{cases} 0, & \mathbf{w} \in \mathcal{B}_\eta(\tilde{\mathbf{Y}}), \\ \infty & \text{otherwise.} \end{cases}$$

Let us define functions $f_1 : \mathbb{R}^{(d^2+1)\tilde{L}} \rightarrow \mathbb{R}$ and $f_2 : \mathbb{R}^{Md\tilde{L}} \rightarrow \mathbb{R}$ by $f_1(\mathbf{s}) := \|\mathbf{s}\|_1$ and $f_2(\mathbf{s}) := \mathbb{1}_{\mathcal{B}_\eta(\tilde{\mathbf{Y}})}(\mathbf{s})$ and introduce the corresponding *Moreau proximal mappings* $\Psi_{\tau f_1} : \mathbb{R}^{(d^2+1)\tilde{L}} \rightarrow \mathbb{R}^{(d^2+1)\tilde{L}}$ and $\Psi_{\tau f_2} : \mathbb{R}^{Md\tilde{L}} \rightarrow \mathbb{R}^{Md\tilde{L}}$ by

$$\begin{aligned} \Psi_{\tau f_1}(\mathbf{s}) &:= \arg \min_{\mathbf{v}} \frac{1}{2} \|\mathbf{v} - \mathbf{s}\|_2^2 + \tau \|\mathbf{v}\|_1, \\ \Psi_{\tau f_2}(\mathbf{s}) &:= \arg \min_{\mathbf{w}} \tau \mathbb{1}_{\mathcal{B}_\eta(\tilde{\mathbf{Y}})}(\mathbf{w}) + \frac{1}{2} \|\mathbf{w} - \mathbf{s}\|_2^2. \end{aligned}$$

Refer, for instance, to [19] and references cited therein for details on Moreau proximal mappings. It is reminded that $\Psi_{\tau f_1}$ with f_1 denoting the l_1 –regularizer turns out to be simply a soft thresholding [1], that is,

$$\Psi_{\tau f_1}(\mathbf{s}) = \text{soft}(\mathbf{s}, \tau),$$

where $\text{soft}(\mathbf{s}, \tau)$ reflects the component-wise operation

$$[\mathbf{s}]_j = \text{sign}([\mathbf{s}]_j) \max\{|[\mathbf{s}]_j| - \tau, 0\}.$$

In numerical implementation, the regularization parameter τ is chosen to be $\tau = 0.1|\tilde{\mathbf{3}}_0|$, where $|\tilde{\mathbf{3}}_0|$ is the average value of $|\mathbf{3}|$ at the zeroth iteration in Algorithm 2. The threshold parameter η is fixed at $\eta = 0.3\|\tilde{\mathbf{Y}}\|_2$. The data fidelity parameter $\tilde{\zeta}$ is manually selected as the optimal

choice from the set $\{8, 4, 2, 1, 1/2, 1/4, 1/8\}$. The parameters θ_{\min} and θ_{\max} in (5.11) are set to $-\infty$ and $+\infty$, respectively. Even in this (unconstrained) setup, the constraint in (5.11) is necessary to introduce additional variable splitting, which allows much faster convergence. This type of additional splitting is quite often used in ADMM. Finally, the relative change of the cost function in (5.10) is used as a stopping criterion, that is, the algorithm is executed until $|(C_k - C_{k-1})/C_k| < 10^{-4}$ is satisfied, where C_k is the cost function at the k -th iteration. With these choices of parameters, the relevant pseudo-code implementation of C-SALSA for the resolution of the unconstrained problem (5.12) is provided in Algorithm 2.

Algorithm 2 C-SALSA for parameter recovery in elasticity imaging.

- 1: Set $k = 0$, choose $\tau > 0$.
 - 2: Set $\mathbf{a}_0^{(i)} = \mathbf{b}_0^{(i)} = 0$, for $i = 1, 2$.
 - 3: **repeat**
 - 4: $\mathbf{r}_k = \tilde{\zeta}(\mathbf{a}_k^{(1)} + \mathbf{b}_k^{(1)}) + \tilde{\Pi}^*(\mathbf{a}_k^{(2)} + \mathbf{b}_k^{(2)})$
 - 5: $\mathbf{z}_{k+1} = \left[(1 + \tilde{\zeta}^2)\mathbf{I} + \tilde{\Pi}^*\tilde{\Pi} \right]^{-1} \mathbf{r}_k$
 - 6: $\mathbf{a}_{k+1}^{(1)} = \Psi_{\tau f_1}(\tilde{\zeta}\mathbf{z}_{k+1} - \mathbf{b}_k^{(1)})$
 - 7: $\mathbf{a}_{k+1}^{(2)} = \Psi_{f_2}(\tilde{\Pi}\mathbf{z}_{k+1} - \mathbf{b}_k^{(2)})$
 - 8: $\mathbf{b}_{k+1}^{(1)} = \mathbf{b}_k^{(1)} - \tilde{\zeta}\mathbf{z}_{k+1} + \mathbf{a}_{k+1}^{(1)}$
 - 9: $\mathbf{b}_{k+1}^{(2)} = \mathbf{b}_k^{(2)} - \tilde{\Pi}\mathbf{z}_{k+1} + \mathbf{a}_{k+1}^{(2)}$
 - 10: $k \leftarrow k + 1$
 - 11: **until** some stopping criterion is satisfied
-

6 Numerical validation of reconstruction scheme

In this section we perform some numerical experiments to validate the proposed reconstruction scheme. We first provide the details of the numerical scheme for the forward model in Section 6.1. Then the examples of the reconstruction of different inclusions are furnished in Section 6.2.

6.1 Forward solver

In order to solve the forward problem for data acquisition, we mainly use the boundary layer potential technique together with the so-called *Nyström discretization scheme*. Let us briefly fix the ideas about the resolution of the forward problem. For simplicity, a two-dimensional case is considered. Note that the vector space Ψ in two-dimensions is given by

$$\Psi = \text{Span} \left\{ \begin{pmatrix} 1 \\ 0 \end{pmatrix}, \begin{pmatrix} 0 \\ 1 \end{pmatrix}, \begin{pmatrix} x_2 \\ -x_1 \end{pmatrix} \right\}.$$

For M distinct points $\mathbf{z}_1, \dots, \mathbf{z}_M \in \mathbb{R}^2 \setminus \overline{\Omega}$, we generate

$$\mathbf{U}_m(\mathbf{x}) = \mathbf{\Gamma}(\mathbf{x} - \mathbf{z}_m) \cdot \begin{pmatrix} 1 \\ 0 \end{pmatrix} + \alpha_1 \begin{pmatrix} 1 \\ 0 \end{pmatrix} + \alpha_2 \begin{pmatrix} 0 \\ 1 \end{pmatrix} + \alpha_3 \begin{pmatrix} x_2 \\ -x_1 \end{pmatrix}, \quad (6.1)$$

where $\alpha_1, \alpha_2, \alpha_3 \in \mathbb{R}$ are chosen so that $\mathbf{U}_m|_{\partial\Omega} \in L^2_{\Psi}(\partial\Omega)$, that is,

$$\int_{\partial\Omega} \mathbf{U}_m \cdot \begin{pmatrix} 1 \\ 0 \end{pmatrix} d\sigma = \int_{\partial\Omega} \mathbf{U}_m \cdot \begin{pmatrix} 0 \\ 1 \end{pmatrix} d\sigma = \int_{\partial\Omega} \mathbf{U}_m \cdot \begin{pmatrix} x_2 \\ -x_1 \end{pmatrix} d\sigma = 0$$

and calculate the surface traction \mathbf{g}_m , for $m = 1, \dots, M$, by $\mathbf{g}_m = \partial \mathbf{U}_m / \partial \boldsymbol{\nu}|_{\partial \Omega}$. Remark that $\mathcal{L}_{\lambda_0, \mu_0}[\mathbf{U}_m] = 0$ in Ω and consequently $\mathbf{g}_m \in L^2_\Psi(\partial \Omega)$.

In order to generate the displacement field \mathbf{u}_m in the presence of inclusions D_1, \dots, D_N , we solve the transmission problem (2.3) using a layer potential technique. Towards this end, we introduce the single layer potential associated to the linear elasticity operator $\mathcal{L}_{\lambda_0, \mu_0}$ by

$$\mathcal{S}_\Omega[\boldsymbol{\varphi}](\mathbf{x}) := \int_{\partial \Omega} \boldsymbol{\Gamma}(\mathbf{x} - \mathbf{y}) \cdot \boldsymbol{\varphi}(\mathbf{y}) d\sigma(\mathbf{y}), \quad \mathbf{x} \in \mathbb{R}^2$$

for all $\boldsymbol{\varphi} \in L^2(\partial \Omega)^2$. It is well known (see, for instance, [22]) that $\mathcal{S}_\Omega[\boldsymbol{\varphi}]$ satisfies the jump relations

$$\frac{\partial}{\partial \boldsymbol{\nu}} \mathcal{S}_\Omega[\boldsymbol{\varphi}] \Big|_{\pm}(\mathbf{x}) = \left(\pm \frac{1}{2} \mathcal{I} + \mathcal{K}_\Omega^* \right) \boldsymbol{\varphi}(\mathbf{x}) \quad \text{a.e. } \mathbf{x} \in \partial \Omega,$$

where \mathcal{K}_Ω^* is the L^2 -adjoint operator of \mathcal{K}_Ω and is defined by

$$\mathcal{K}_\Omega^*[\boldsymbol{\varphi}](\mathbf{x}) := \text{p.v.} \int_{\partial \Omega} \frac{\partial}{\partial \boldsymbol{\nu}_{\mathbf{x}}} \boldsymbol{\Gamma}(\mathbf{x} - \mathbf{y}) \cdot \boldsymbol{\varphi}(\mathbf{y}) d\sigma(\mathbf{y}), \quad \text{a.e. } \mathbf{x} \in \partial \Omega$$

for all $\boldsymbol{\varphi} \in L^2(\partial \Omega)^2$. Then, the solution to the transmission problem (2.3) can be represented as (see, for instance, [6, Theorem 6.15])

$$\mathbf{u}_m(\mathbf{x}) = \begin{cases} \mathcal{S}_\Omega[\boldsymbol{\eta}_m] + \mathcal{S}_D[\boldsymbol{\psi}_m](\mathbf{x}), & \text{if } \mathbf{x} \in \Omega \setminus \overline{D} \\ \tilde{\mathcal{S}}_D[\boldsymbol{\varphi}_m](\mathbf{x}), & \mathbf{x} \in D, \end{cases} \quad (6.2)$$

where the triplet $(\boldsymbol{\varphi}_m, \boldsymbol{\psi}_m, \boldsymbol{\eta}_m) \in L^2(\partial D)^2 \times L^2_\Psi(\partial \Omega)^2 \times L^2(\partial D)^2$ is the unique solution to the integral system

$$\begin{bmatrix} \tilde{\mathcal{S}}_D|_{\partial D} & -\mathcal{S}_D|_{\partial D} & -\mathcal{S}_\Omega|_{\partial D} \\ \left(-\frac{1}{2}I + \tilde{\mathcal{K}}_D^* \right) & -\left(\frac{1}{2}I + \mathcal{K}_D^* \right) & -\frac{\partial}{\partial \boldsymbol{\nu}} \mathcal{S}_\Omega|_{\partial D} \\ 0 & \frac{\partial}{\partial \boldsymbol{\nu}} \mathcal{S}_D|_{\partial \Omega} & \left(-\frac{1}{2}I + \mathcal{K}_\Omega^* \right) \end{bmatrix} \begin{bmatrix} \boldsymbol{\varphi}_m \\ \boldsymbol{\psi}_m \\ \boldsymbol{\eta}_m \end{bmatrix} = \begin{bmatrix} 0 \\ 0 \\ \mathbf{g}_m \end{bmatrix}, \quad (6.3)$$

subject to the constraint $\mathbf{u}_m \in L^2_\Psi(\partial \Omega)$, thanks to the transmission and the boundary conditions. Here $\tilde{\mathcal{S}}_D$ and $\tilde{\mathcal{K}}_D^*$ are the operators related to the parameters (λ, μ) .

Our aim is to solve the system (6.3) for $(\boldsymbol{\varphi}_m, \boldsymbol{\psi}_m, \boldsymbol{\eta}_m)$ and then evaluate $\mathbf{u}_m|_{\partial \Omega}$ using representation (6.2). In order to numerically solve system (6.3), we express \mathcal{K}_Ω^* as

$$\mathcal{K}_\Omega^*[\mathbf{f}](\mathbf{x}) = \text{p.v.} \int_0^1 \frac{\partial}{\partial \boldsymbol{\nu}_{\mathbf{x}}} \boldsymbol{\Gamma}(\mathbf{x} - \mathbf{x}(t)) \cdot \mathbf{f}(\mathbf{x}(t)) |\mathbf{x}'(t)| dt, \quad \mathbf{x} \in \partial D, \quad (6.4)$$

where $x(t)$ is a parametrization of $\partial \Omega$. Then the Nyström discretization, with P boundary points $\{\mathbf{x}_p\}_{p=1}^P$ and weight w_p , renders

$$\mathcal{K}_\Omega^*[\mathbf{f}](\mathbf{x}) \approx \sum_{p=1}^P \frac{\partial}{\partial \boldsymbol{\nu}_{\mathbf{x}}} \boldsymbol{\Gamma}(\mathbf{x} - \mathbf{x}_p) \cdot \mathbf{f}_p |\mathbf{x}'_p| w_p, \quad \mathbf{x} \in \partial \Omega, \quad (6.5)$$

where $\mathbf{f}_p = \mathbf{f}(\mathbf{x}_p)$ for $p = 1, \dots, P$. Here, the simplest quadrature rule

$$\int_0^1 \mathbf{f}(t) dt \approx \sum_{p=1}^P \frac{1}{P} \mathbf{f}\left(\frac{p}{P}\right)$$

is used. It is emphasized that the integral (6.4) is defined as the Cauchy principal value. Thus, the singularity of $\partial[\Gamma(\mathbf{x} - \mathbf{x}_p)]/\partial\boldsymbol{\nu}_{\mathbf{x}}$ at $\mathbf{x} = \mathbf{x}_p$ should be evaluated in the sense of Cauchy principle value. The numerical computation of \mathcal{K}_{Ω}^* can be realized using (6.5). Similarly, we can discretize \mathcal{K}_{Ω} , \mathcal{S}_{Ω} and \mathcal{D}_{Ω} as

$$\begin{aligned}\mathcal{K}_{\Omega}[\mathbf{f}](\mathbf{x}) &\approx \sum_{p=1}^P \frac{\partial}{\partial\boldsymbol{\nu}(\mathbf{x}_p)} \Gamma(\mathbf{x} - \mathbf{x}_p) \cdot \mathbf{f}_p |\mathbf{x}'_p| w_p, \quad \mathbf{x} \in \partial\Omega, \\ \mathcal{S}_{\Omega}[\mathbf{f}](\mathbf{x}) &\approx \sum_{p=1}^P \Gamma(\mathbf{x} - \mathbf{x}_p) \cdot \mathbf{f}_p |\mathbf{x}'_p| w_p, \quad \mathbf{x} \in \Omega, \\ \mathcal{D}_{\Omega}[\mathbf{f}](\mathbf{x}) &\approx \sum_{p=1}^P \frac{\partial}{\partial\boldsymbol{\nu}(\mathbf{x}_p)} \Gamma(\mathbf{x} - \mathbf{x}_p) \cdot \mathbf{f}_p |\mathbf{x}'_p| w_p, \quad \mathbf{x} \in \Omega.\end{aligned}$$

Consequently, the integral system (6.3) can be discretized and solved for $(\boldsymbol{\varphi}_m, \boldsymbol{\psi}_m, \boldsymbol{\eta}_m)$. The preprocessing of the data $(\mathbf{u}_m - \mathbf{U}_m)$ using the Calerón preconditioner $(-1/2\mathcal{I} + \mathcal{K}_{\Omega})$ can be realized in the similar fashion using discretization of the Neumann Poincaré operator \mathcal{K}_{Ω} .

6.2 Numerical experiments

For numerical examples, let the background domain Ω to be an ellipse of semi-major and semi-minor axes $10mm$ and $7mm$ respectively with shear and compression moduli $\mu_0 = \lambda_0 = 1GPa$. Three different kinds of inclusions are considered for numerical experiments. Precisely, the examples of sparse, extended and thin or worm-like inclusions are taken into account. The sparse inclusions are modeled with three unit disks. The extended inclusion is modeled with a non-convex kite shaped domain with the size comparable to that of the background domain in order of magnitude. By thin or worm-like inclusions we mean that one dimension of the inclusions is much smaller than the other dimension. The examples of straight and curved thin inclusions are dealt with. The test geometries are delineated in Figure 2. The field of view is discretized to have a grid size $1/3mm$ for all reconstructions. The Lamé parameters of the three inclusions in the sparse case are both fixed at $7GPa$ for the leftmost inclusion, $2GPa$ for the inclusion in the middle, and $2.5GPa$ for the rightmost inclusion. For the rest of the examples, the Lamé parameters of the targets are both fixed at $2GPa$.

6.2.1 Parameter selection

In order to generate measurements, we choose $M = 4$. Accordingly, points $\mathbf{z}_1 = (12, 11)$, $\mathbf{z}_2 = (9, -11)$, $\mathbf{z}_3 = (-1, 8)$ and $\mathbf{z}_4 = (-50, 0)$ are chosen to get background fields \mathbf{U}_m using (6.1) and the corresponding boundary traction forces $\{\mathbf{g}_m\}_{m=1}^4$ resulting therefrom. The forward data is acquired using the forward solver described in Section 6.1. $P = 2000$ discretization points on $\partial\Omega$ and ∂D_n , for each n , are used for the example of sparse inclusions and $P = 5000$ points are used for rest of the examples. Three different sets of the full aperture sampled measurement points $\{\mathbf{x}_r\}_{r=1}^R$ with $R = 100, 32, 16$ and a set of limited view sampled measurement points on $\partial\Omega$ with $R = 16$ are taken into account. The latter case is indicated hereinafter by $R = 16p$. The measurement setups are depicted in Figure 3. An additive Gaussian noise with signal-to-noise ratio $40dB$ was added to the boundary measurement vectors $(\mathbf{u}_m - \mathbf{U}_m)|_{\partial\Omega}$ for all simulations.

In order to recover the density \mathfrak{X} over the support \hat{D} , the modified M-SBL Algorithm 1 is applied on the preconditioned problem (5.8) using regularization parameter $\theta = 10^{-2} \times \sigma_{\max}^2$,

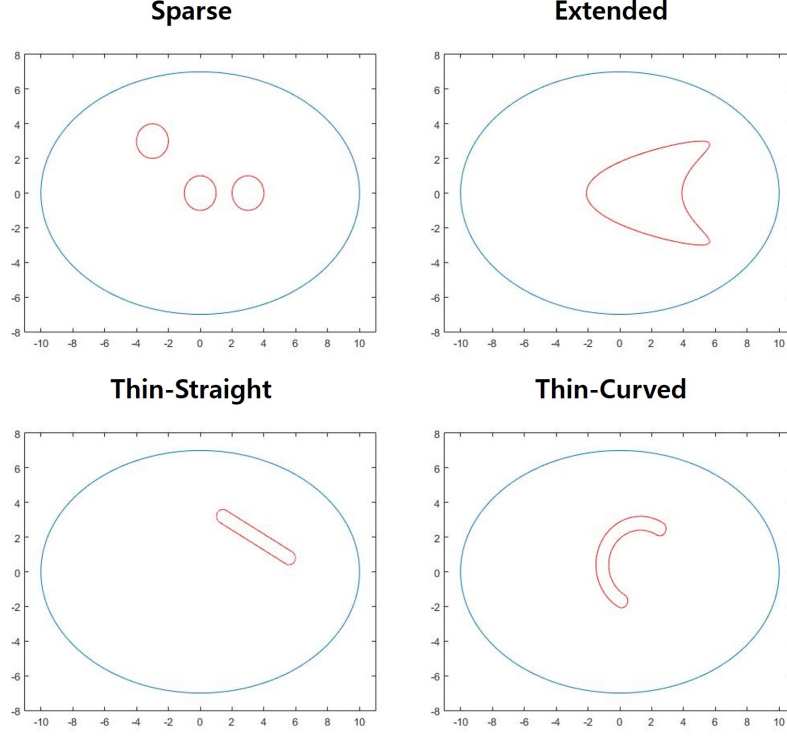


Figure 2: Geometric configuration and different test inclusions.

where σ_{\max} denotes the maximum singular value of the sensing matrix Π . The threshold parameter ϱ in Algorithm 1 is set to be $\varrho = 10^{-3}$.

For support identification, the pruning parameter ξ in (5.9) is set to be $\xi = 0$, that is, we do not prune small values and fully utilize the obtained information in order to avoid a sub-optimal selection of ξ . The box constraint parameters θ_{\min} and θ_{\max} in (5.11) are set to be very large so that we can simply assume $[\mathbf{3}]_i \in (-\infty, +\infty)$.

The selected optimal values of the parameters for Algorithms 1-2 are summarized in Table 1. These parameters are used for all examples except for data fidelity parameter $\tilde{\zeta}$, which is gradually decreased in value with respect to the decrease in the number of measurement points.

6.2.2 Simulation results

The reconstructed shear and compression moduli for different inclusions together with estimated support of the inclusions are provided in Figures 4-7 for sparse, thin straight, thin curved and extended inclusions respectively. For all the listed inclusions, the results are furnished with different configurations of measurement points (with $R = 100, 32, 16, 16p$) as precised earlier. When $R = 100$, the proposed algorithm clearly recovered the structures of the inclusions and their constitutive parameters in all cases. For instance, for sparse inclusions, even though the parameter values have been varied by tuning the optimization parameters, their relative

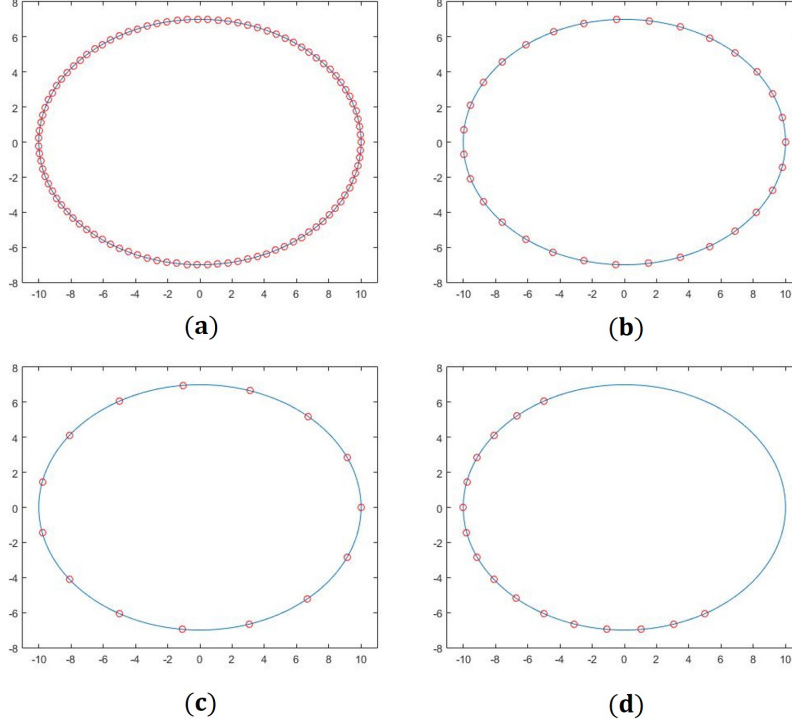


Figure 3: Configuration of the measurement points on the boundary of Ω . (a) $R = 100$. (b) $R = 32$. (c) $R = 16$. (d) $R = 16p$.

Proposed Method	Sparse target	Thin-Straight target	Thin-Curved target	Extended target
Step 1: M-SBL	Iter _{max} = 50 with preconditioning	Iter _{max} = 50 with preconditioning	Iter _{max} = 50 with preconditioning	Iter _{max} = 50 with preconditioning
Step 2: C-SALSA	$\tau = 0.1 \tilde{\mathbf{z}}_0 $ $\eta = 0.3\ \tilde{\mathbf{Y}}\ _2$ $\tilde{\zeta} = 2$ ($R = 100$) $\tilde{\zeta} = 1/2$ ($R = 32$) $\tilde{\zeta} = 1/4$ ($R = 16$) $\tilde{\zeta} = 1/4$ ($R = 16p$)	$\tau = 0.1 \tilde{\mathbf{z}}_0 $ $\eta = 0.3\ \tilde{\mathbf{Y}}\ _2$ $\tilde{\zeta} = 4$ ($R = 100$) $\tilde{\zeta} = 2$ ($R = 32$) $\tilde{\zeta} = 1$ ($R = 16$) $\tilde{\zeta} = 1/2$ ($R = 16p$)	$\tau = 0.1 \tilde{\mathbf{z}}_0 $ $\eta = 0.3\ \tilde{\mathbf{Y}}\ _2$ $\tilde{\zeta} = 4$ ($R = 100$) $\tilde{\zeta} = 1$ ($R = 32$) $\tilde{\zeta} = 1/2$ ($R = 16$) $\tilde{\zeta} = 1/2$ ($R = 16p$)	$\tau = 0.1 \tilde{\mathbf{z}}_0 $ $\eta = 0.3\ \tilde{\mathbf{Y}}\ _2$ $\tilde{\zeta} = 8$ ($R = 100$) $\tilde{\zeta} = 4$ ($R = 32$) $\tilde{\zeta} = 2$ ($R = 16$) $\tilde{\zeta} = 2$ ($R = 16p$)

Table 1: Parameters choices for numerical simulations.

relationships remained same so that the leftmost inclusion always appears to have the highest value and the middle one has the lowest value (see Figure 4). It is observed that the overall reconstruction performance gradually suffers when the number of measurement points decreases. Nevertheless, the results corresponding to $R = 32$ are comparable to those of $R = 100$. Even when $R = 16$, the simulations are able to indicate the crude shapes of inclusions. However, when the measurement points only cover the partial aperture ($R = 16p$), the results are distorted. The reconstructions for thin and extended targets show comparatively less accurate results

than those for the sparse targets. Indeed, the support set of the inclusion is not very sparse inside the background domain. It is worthwhile to mention that M-SBL is able to localize the anomalies even in the deteriorated conditions. In deteriorated cases, although the M-SBL algorithm recovered the locations outside the expected regions, the estimated M-SBL values are relatively higher inside and near the boundary of the inclusions than spurious detected region outside the inclusions (see Figure 8). The points outside the inclusions with small values can be easily filtered by appropriately tuning the pruning parameter ξ .

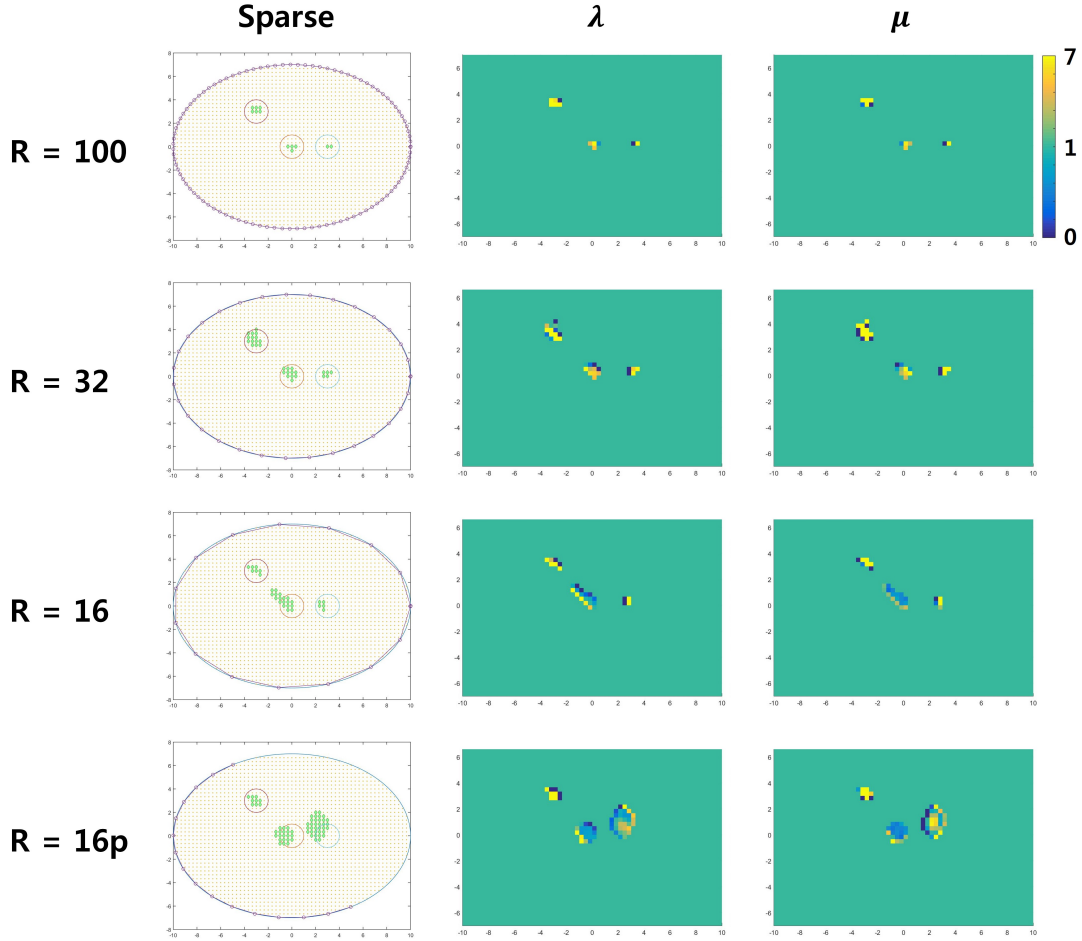


Figure 4: Reconstruction of multiple disk-like inclusions. Left to Right: \hat{D} , λ , and μ .

7 Conclusion

A joint sparse recovery based direct algorithm was proposed to reconstruct the spatial support of multiple elastic inclusions and their material parameters using only a few measurements of the displacement over a very coarse grid of boundary points (in the sense of Nyquist sampling

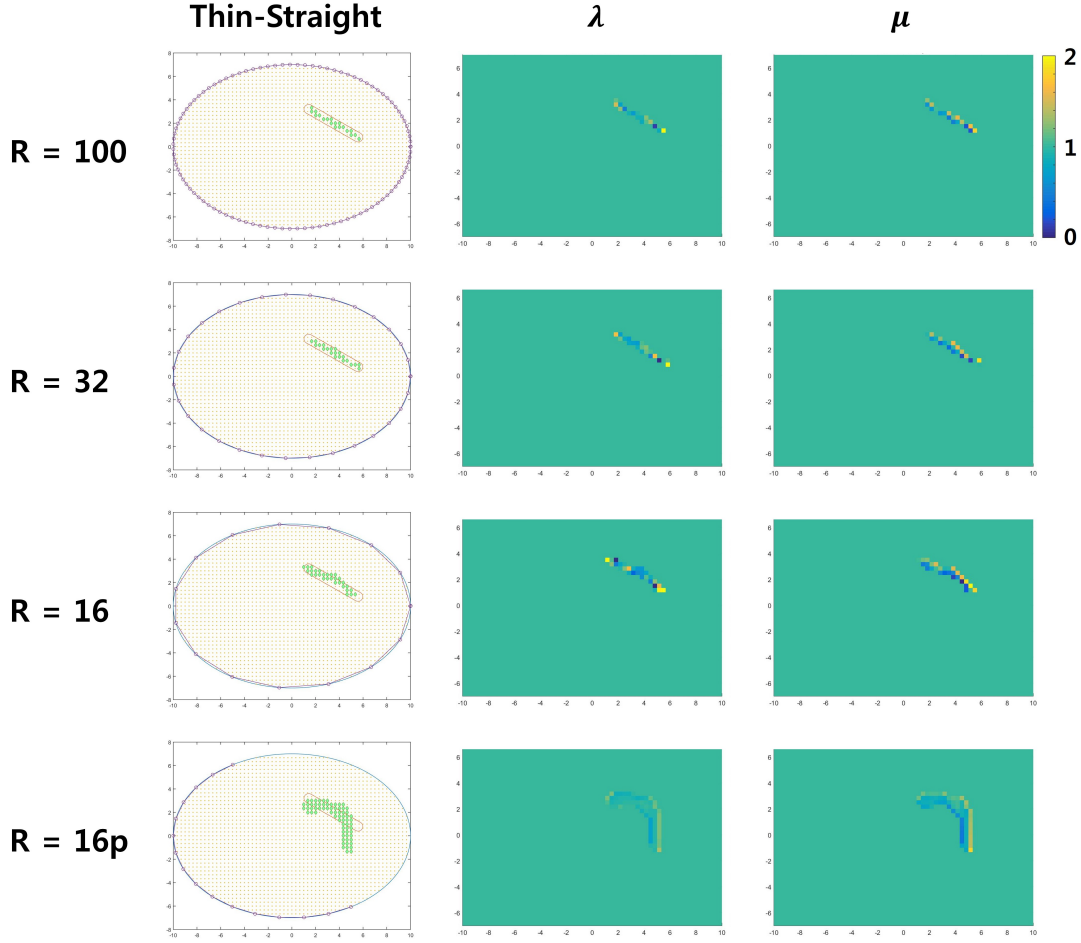


Figure 5: Reconstruction of a thin-straight inclusion. Left to Right: \hat{D} , λ , and μ .

rate). The inverse problem for support detection was converted to a joint sparse recovery problem for internal data (linked to the displacement and strain fields inside the support set of inclusions) by virtue of an integral formulation. The sparse signal recovery problem resulting therefrom was resolved for an exact and unique solution by invoking a modified M-SBL algorithm with structural constraints. Then, using the leverage of the learned internal information about the displacement field, a linear inverse problem for quantitative evaluation of material parameters was formulated. This resulting problem was then converted to a noise robust constraint optimization problem, which was subsequently solved using the C-SALSA. The proposed imaging algorithm was computationally very efficient and was felicitous to demonstrate very accurate reconstruction since it is non-iterative and does not require any linearization or computations of multiple forward solutions. The advantage is taken here of the learned internal data and the sparsity of the support set of the inclusions inside the elastic medium to reduce the mathematical ill-posedness of the underlying inverse problem. In fact, the recovery of such an

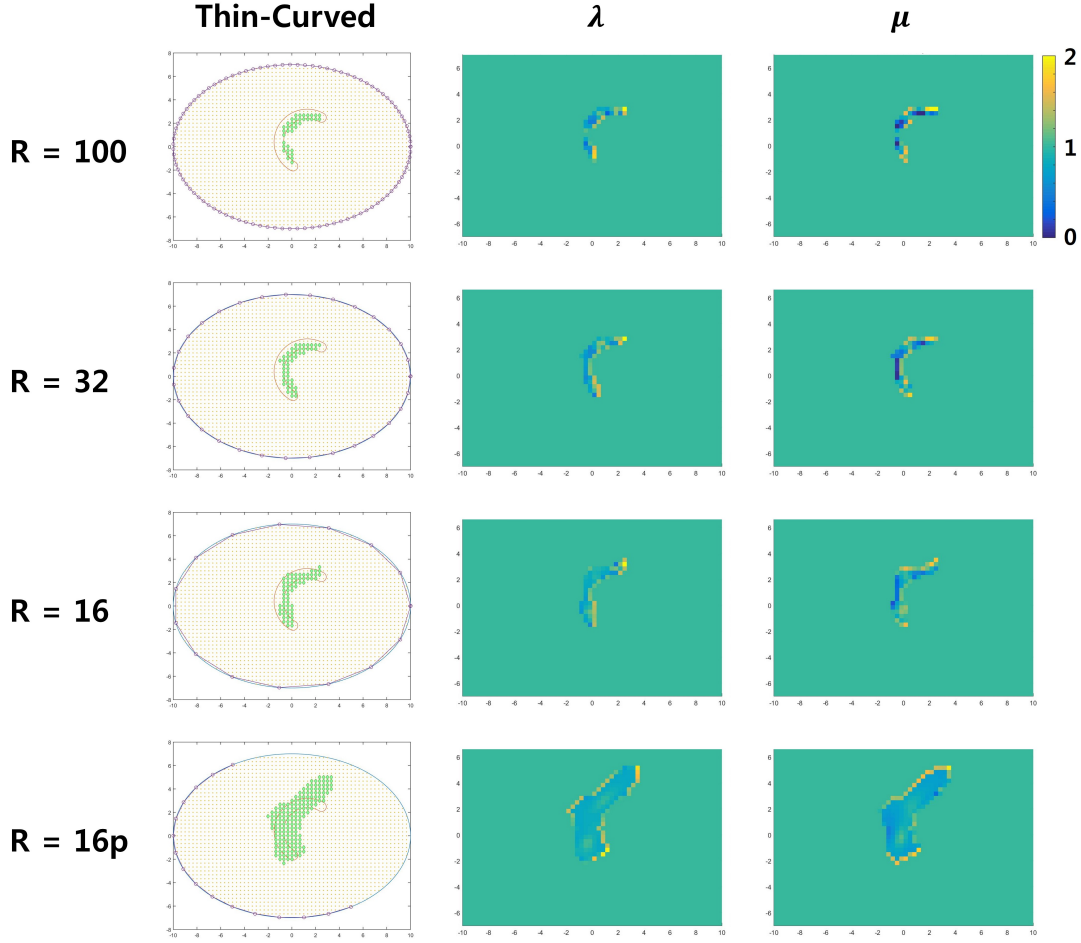


Figure 6: Reconstruction of a thin-curved inclusion. Left to Right: \hat{D} , λ , and μ .

information is very novel and pertinent. This additional information compensate for the under-determined data and therefore renders stability to the reconstruction framework. In addition, since no linearization or simplifying approximations are used, the proposed technique provides reconstruction with better resolution and quality than classical techniques. However, a more sophisticated quantitative mathematical analysis is certainly necessary in order to ascertain the stability and resolution properties of the proposed framework in terms of the relative size of the inclusion, the number of measurement fields, the number and the placement of the measurement points on the boundary and the aperture size. This will be the subject of future investigations. Albeit, the elastostatic problem is undertaken in this article, the quasi-static or time-harmonic elasticity problems are also amenable to the same treatment with minor changes. Moreover, the elasticity imaging problem in the so-called quasi-incompressible regime can also be dealt with and will be investigated in future.

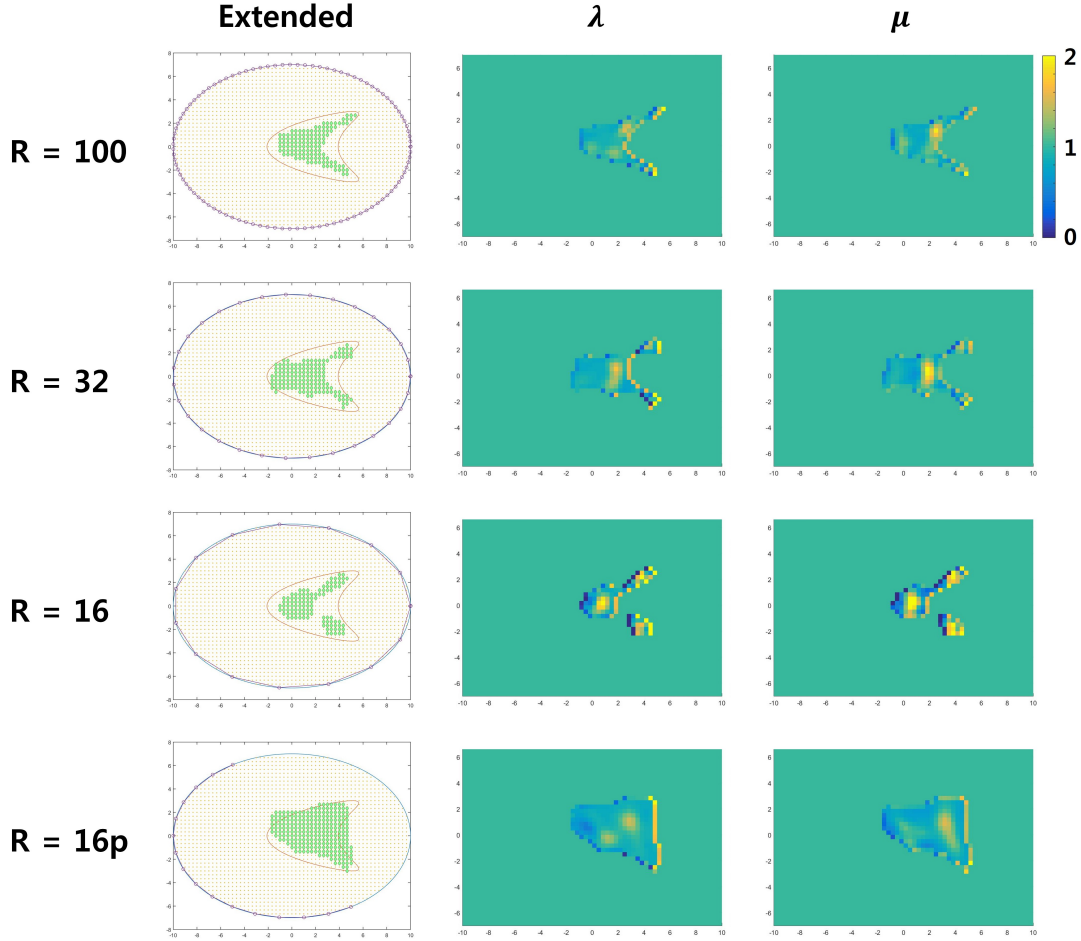


Figure 7: Reconstruction of an extended inclusion. Left to Right: \hat{D} , λ , and μ .

A Evaluation of integral kernels

Let us provide the explicit expressions for different kernels involved in our integral formulation and those required to compute the sensing matrix of the reconstruction framework. For brevity we restrict ourselves to two dimensional case only.

Following identities will be handy in ensuing calculations. For all $\mathbf{x}, \mathbf{y} \in \mathbb{R}^2$ such that $\mathbf{x} \neq \mathbf{y}$ and $i, j \in \{1, 2\}$

$$\begin{cases} \frac{\partial}{\partial y_i} \ln |\mathbf{x} - \mathbf{y}| = -\frac{x_i - y_i}{|\mathbf{x} - \mathbf{y}|^2}, \\ \frac{\partial^2}{\partial y_i \partial y_j} \ln |\mathbf{x} - \mathbf{y}| = -2 \frac{(x_i - y_i)(x_j - y_j)}{|\mathbf{x} - \mathbf{y}|^4} + \delta_{ij} \frac{1}{|\mathbf{x} - \mathbf{y}|^2}, \\ \Delta_{\mathbf{y}} \ln |\mathbf{x} - \mathbf{y}| = 0. \end{cases} \quad (\text{A.1})$$

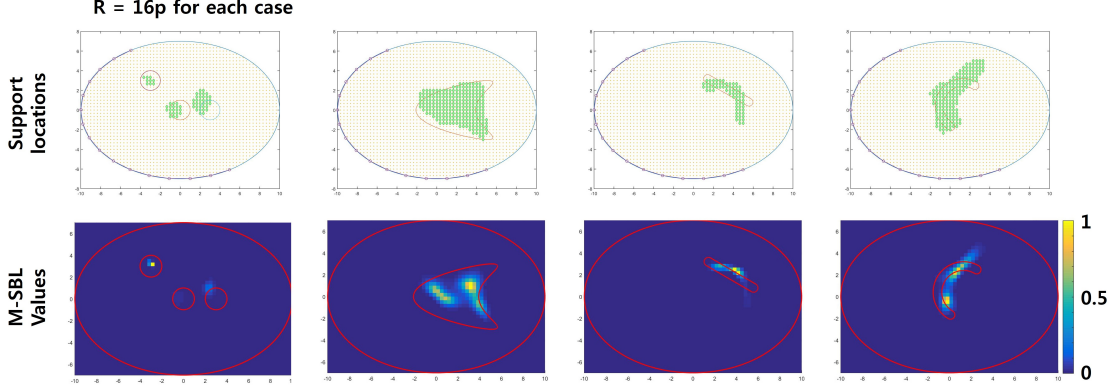


Figure 8: Support identification using M-SBL in deteriorated cases. Top: Reconstructed support sets. Bottom: The normalized M-SBL values $\psi_\ell / \max_{i \in \{1, \dots, L\}}(\psi_i)$.

A.1 Surface traction of Kelvin matrix and boundary integral operators

We first recall the expression of the surface traction of $\mathbf{\Gamma}$ whose derivation can be found in [7, Appendix A]. For all $\mathbf{x}, \mathbf{y} \in \mathbb{R}^2$, $\mathbf{x} \neq \mathbf{y}$, we have

$$\begin{aligned} \left(\frac{\partial \mathbf{\Gamma}}{\partial \boldsymbol{\nu}_{\mathbf{y}}}(\mathbf{x}, \mathbf{y}) \right)_{ij} &= \left[a \delta_{ij} + b \frac{(x_i - y_i)(x_j - y_j)}{|\mathbf{x} - \mathbf{y}|^2} \right] \left(\sum_{k=1}^2 \frac{\nu_k(x_k - y_k)}{|\mathbf{x} - \mathbf{y}|^2} \right) \\ &\quad - a \frac{\nu_j(x_i - y_i) - \nu_i(x_j - y_j)}{|\mathbf{x} - \mathbf{y}|^2}, \quad i, j \in \{1, 2\}, \end{aligned} \quad (\text{A.2})$$

where

$$\nu_i = [\boldsymbol{\nu}]_i, \quad a := -\frac{\mu_0}{2\pi(\lambda_0 + 2\mu_0)} \quad \text{and} \quad b := -\frac{\lambda_0 + \mu_0}{\pi(\lambda_0 + 2\mu_0)}.$$

Therefore, thanks to (A.2), the boundary integral operators \mathcal{S}_Ω , \mathcal{D}_Ω and \mathcal{K}_Ω can be evaluated as

$$\begin{aligned} \mathcal{S}_\Omega[\boldsymbol{\varphi}](\mathbf{x}) &:= \left(\sum_{i,j=1}^2 \int_{\partial\Omega} [\mathbf{\Gamma}(\mathbf{x} - \mathbf{y})]_{ij} \cdot [\boldsymbol{\varphi}(\mathbf{y})]_j d\sigma(\mathbf{y}) \right) \mathbf{e}_i, \quad \mathbf{x} \in \mathbb{R}^d \setminus \partial\Omega, \\ \mathcal{D}_\Omega[\boldsymbol{\varphi}](\mathbf{x}) &:= \left(\sum_{i,j=1}^2 \int_{\partial\Omega} \left[\frac{\partial}{\partial \boldsymbol{\nu}_{\mathbf{y}}} \mathbf{\Gamma}(\mathbf{x} - \mathbf{y}) \right]_{ij} \cdot [\boldsymbol{\varphi}(\mathbf{y})]_j d\sigma(\mathbf{y}) \right) \mathbf{e}_i, \quad \mathbf{x} \in \mathbb{R}^d, \\ \mathcal{K}_\Omega[\boldsymbol{\varphi}](\mathbf{x}) &:= \left(\sum_{i,j=1}^2 \text{p.v.} \int_{\partial\Omega} \left[\frac{\partial}{\partial \boldsymbol{\nu}_{\mathbf{y}}} \mathbf{\Gamma}(\mathbf{x} - \mathbf{y}) \right]_{ij} \cdot [\boldsymbol{\varphi}(\mathbf{y})]_j d\sigma(\mathbf{y}) \right) \mathbf{e}_i, \quad \text{a.e. } \mathbf{x} \in \partial\Omega \end{aligned}$$

for all $\boldsymbol{\varphi} \in L^2_\Psi(\partial\Omega)$.

A.2 Divergence of Kelvin matrix

We remind that (see, for instance, [2, Lemma 3.3.2])

$$\nabla_{\mathbf{y}} \cdot \mathbf{\Gamma}(\mathbf{x}, \mathbf{y}) = \frac{1}{(\lambda_0 + 2\mu_0)} \nabla_{\mathbf{y}} \Phi(\mathbf{x}, \mathbf{y}) = \frac{1}{(\lambda_0 + 2\mu_0)} \sum_{i=1}^2 \frac{\partial}{\partial y_i} \Phi(\mathbf{x}, \mathbf{y}) \mathbf{e}_i, \quad (\text{A.3})$$

where $\Phi(\mathbf{x}, \cdot) : \mathbb{R}^2 \rightarrow \mathbb{R}$, for fixed $\mathbf{x} \in \mathbb{R}^2$, is the fundamental solution to the Laplace equation in \mathbb{R}^2 , that is,

$$\Delta_{\mathbf{y}} \Phi(\mathbf{x}, \mathbf{y}) = -\delta_{\mathbf{x}}(\mathbf{y}), \quad \forall \mathbf{x}, \mathbf{y} \in \mathbb{R}^2$$

and is given by

$$\Phi(\mathbf{x}, \mathbf{y}) = \frac{1}{2\pi} \ln |\mathbf{x} - \mathbf{y}|, \quad \forall \mathbf{x}, \mathbf{y} \in \mathbb{R}^2, \quad \mathbf{x} \neq \mathbf{y}.$$

Thus, after fairly easy manipulations and using identities (A.1) in (A.3), one arrives at

$$\nabla_{\mathbf{y}} \cdot \mathbf{\Gamma}(\mathbf{x}, \mathbf{y}) = \frac{a}{\mu_0} \sum_{i=1}^2 \frac{(x_i - y_i)}{|\mathbf{x} - \mathbf{y}|^2} \mathbf{e}_i, \quad \mathbf{x}, \mathbf{y} \in \mathbb{R}^2 \quad \mathbf{x} \neq \mathbf{y}.$$

A.3 Strain of Kelvin matrix

Let us calculate $\left[\mathcal{E}[\mathbf{\Gamma}(\mathbf{x}, \cdot)](\mathbf{y}) \right]_{ijk}$ for $d = 2$. In this case we can express $\mathbf{\Gamma}$ as

$$\gamma_{ij}(\mathbf{x} - \mathbf{y}) = \alpha \delta_{ij} \ln |\mathbf{x} - \mathbf{y}| + \beta (x_i - y_i) \frac{\partial}{\partial y_j} \ln |\mathbf{x} - \mathbf{y}|, \quad \mathbf{x}, \mathbf{y} \in \mathbb{R}^2, \quad \mathbf{x} \neq \mathbf{y},$$

where α and β are given by (3.1). Therefore,

$$\begin{aligned} & \frac{\partial}{\partial y_k} \gamma_{ij}(\mathbf{x} - \mathbf{y}) \\ &= \alpha \delta_{ij} \frac{\partial}{\partial y_k} \ln |\mathbf{x} - \mathbf{y}| + \beta \frac{\partial}{\partial y_k} (x_i - y_i) \frac{\partial}{\partial y_j} \ln |\mathbf{x} - \mathbf{y}| + \beta (x_i - y_i) \frac{\partial^2}{\partial y_k \partial y_j} \ln |\mathbf{x} - \mathbf{y}| \\ &= -\alpha \delta_{ij} \frac{(x_k - y_k)}{|\mathbf{x} - \mathbf{y}|^2} + \beta \delta_{ik} \frac{(x_j - y_j)}{|\mathbf{x} - \mathbf{y}|^2} + \beta \delta_{jk} \frac{(x_i - y_i)}{|\mathbf{x} - \mathbf{y}|^2} - 2\beta \frac{(x_i - y_i)(x_j - y_j)(x_k - y_k)}{|\mathbf{x} - \mathbf{y}|^4}. \end{aligned}$$

Consequently, we can calculate $\left[\mathcal{E}[\mathbf{\Gamma}(\mathbf{x}, \cdot)](\mathbf{y}) \right]_{ijk}$ for all $i, j, k \in \{1, 2\}$ as

$$\begin{aligned} 2 \left[\mathcal{E}[\mathbf{\Gamma}(\mathbf{x}, \cdot)](\mathbf{y}) \right]_{ijk} &= \left(\frac{\partial \gamma_{ij}}{\partial y_k}(\mathbf{x}, \mathbf{y}) + \frac{\partial \gamma_{ik}}{\partial y_j}(\mathbf{x}, \mathbf{y}) \right) \\ &= -\alpha \delta_{ij} \frac{(x_k - y_k)}{|\mathbf{x} - \mathbf{y}|^2} + \beta \delta_{ik} \frac{(x_j - y_j)}{|\mathbf{x} - \mathbf{y}|^2} + \beta \delta_{jk} \frac{(x_i - y_i)}{|\mathbf{x} - \mathbf{y}|^2} - 2\beta \frac{(x_i - y_i)(x_j - y_j)(x_k - y_k)}{|\mathbf{x} - \mathbf{y}|^4} \\ &\quad -\alpha \delta_{ik} \frac{(x_j - y_j)}{|\mathbf{x} - \mathbf{y}|^2} + \beta \delta_{ij} \frac{(x_k - y_k)}{|\mathbf{x} - \mathbf{y}|^2} + \beta \delta_{jk} \frac{(x_i - y_i)}{|\mathbf{x} - \mathbf{y}|^2} - 2\beta \frac{(x_i - y_i)(x_j - y_j)(x_k - y_k)}{|\mathbf{x} - \mathbf{y}|^4} \\ &= (\beta - \alpha) \left[\delta_{ij} \frac{(x_k - y_k)}{|\mathbf{x} - \mathbf{y}|^2} + \delta_{ik} \frac{(x_j - y_j)}{|\mathbf{x} - \mathbf{y}|^2} \right] + 2\beta \delta_{jk} \frac{(x_i - y_i)}{|\mathbf{x} - \mathbf{y}|^2} \\ &\quad - 4\beta \frac{(x_i - y_i)(x_j - y_j)(x_k - y_k)}{|\mathbf{x} - \mathbf{y}|^4}. \end{aligned}$$

By remarking that $a = \beta - \alpha$ we finally arrive at

$$\begin{aligned} \left[\mathcal{E}[\mathbf{\Gamma}(\mathbf{x}, \cdot)](\mathbf{y}) \right]_{ijk} = & \frac{a}{2} \left[\delta_{ij} \frac{(x_k - y_k)}{|\mathbf{x} - \mathbf{y}|^2} + \delta_{ik} \frac{(x_j - y_j)}{|\mathbf{x} - \mathbf{y}|^2} \right] + \beta \delta_{jk} \frac{(x_i - y_i)}{|\mathbf{x} - \mathbf{y}|^2} \\ & - 2\beta \frac{(x_i - y_i)(x_j - y_j)(x_k - y_k)}{|\mathbf{x} - \mathbf{y}|^4}. \end{aligned}$$

References

- [1] M. AFONSO, J. BIOUCAS-DIAS, AND M. FIGUEIREDO, *An augmented Lagrangian approach to the constrained optimization formulation of imaging inverse problems*, IEEE Trans. Image Process., 20 (2011), pp. 681–695.
- [2] H. AMMARI, *An Introduction to Mathematics of Emerging Biomedical Imaging*, Math. Appl. (Berlin) 62, Springer-Verlag, Berlin, 2008.
- [3] H. AMMARI, E. BRETIN, J. GARNIER, H. KANG, H. LEE, AND A. WAHAB, *Mathematical Methods in Elasticity Imaging*, Princeton Ser. Appl. Math., Princeton University Press, Princeton, NJ, 2015.
- [4] H. AMMARI, E. BRETIN, J. GARNIER, W. JING, H. KANG, AND A. WAHAB, *Localization, stability, and resolution of topological derivative based imaging functionals in elasticity*, SIAM J. Imaging Sci., 6 (2013), pp. 2174–2212.
- [5] H. AMMARI, P. GARAPON, H. KANG, AND H. LEE, *A method of biological tissues elasticity reconstruction using magnetic resonance elastography measurements*, Quart. Appl. Math., 66 (2008), pp. 139–175.
- [6] H. AMMARI AND H. KANG, *Reconstruction of Small Inhomogeneities from Boundary Measurements*, Lecture Notes in Math. 1846, Springer-Verlag, Berlin, 2004.
- [7] H. AMMARI, H. KANG, H. LEE, AND J. LIM, *Boundary perturbations due to the presence of small linear cracks in an elastic body*, J. Elast., 113 (2013), pp. 75–91.
- [8] J. AN, Y. BIRSEN, A. ANGELIQUE, AND N. VASILIS, *Preconditioning of the fluorescence diffuse optical tomography sensing matrix based on compressive sensing*, Opt. Lett., 37 (2012), pp. 4326–4328.
- [9] G. BAL, C. BELLIS, S. IMPERIALE, AND F. MONARD, *Reconstruction of constitutive parameters in isotropic linear elasticity from noisy full field measurements*, Inverse Probl., 30 (2014), 125004.
- [10] G. BAL AND S. IMPERIALE, *Displacement reconstruction in ultrasound elastography*, SIAM J. Imaging Sci., 8 (2015), pp. 1070–1089.
- [11] G. BAL, F. MONARD, AND G. UHLMANN, *Reconstruction of a fully anisotropic elasticity tensor from knowledge of displacement fields*, SIAM J. Appl. Math., 75 (2015), pp. 2214–2231.
- [12] E. BARBONE AND N. H. GOKHALE, *Elastic modulus imaging: On the uniqueness and nonuniqueness of the elastography inverse problem in two dimensions*, Inverse Probl., 20 (2004), pp. 203–296.

- [13] J. BERGH AND J. LÖFSTRÖM, *Interpolation Spaces. An Introduction*, Grundlehren der Mathematischen Wissenschaften 223, Springer-Verlag, Berlin-New York, 1976.
- [14] M. BONNET AND A. CONSTANTINESCU, *Inverse problems in elasticity*, Inverse Probl., 21 (2005), R1–R50.
- [15] S. AVRIL, M. BONNET, A.-S. BRETTELLE, M. GRÉDIAC, F. HILD, P. IENNY, F. LA-TOURTE, D. LEMOSSE, S. PAGANO, E. PAGNACCO, AND F. PIERRON, *Overview of identification methods of mechanical parameters based on full-field measurements*, Exp. Mech., 48 (2008), pp. 381–402.
- [16] E. CANDÈS, J. ROMBERG, AND T. TAO, *Robust uncertainty principles: Exact signal reconstruction from highly incomplete frequency information*, IEEE Trans. Inf. Theory, 52 (2006), pp. 489–509.
- [17] E. J. CANDÈS AND M. B. WAKIN, *An introduction to compressive sampling*, IEEE Signal Process. Mag., 25 (2008), pp. 21–30.
- [18] J. CHEN AND X. HUO, *Theoretical results on sparse representations of multiple measurement vectors*, IEEE Trans. Signal Process., 54 (2006), pp. 4634–4643.
- [19] P. L. COMBETTES AND V. R. WAJS, *Signal recovery by proximal forward-backward splitting*, SIAM J. Multiscale Model. Sim., 4 (2005), pp. 1168–1200.
- [20] A. CONSTANTINESCU, *On the identification of elastic moduli from displacement force boundary measurements*, Inverse Probl. Eng., 1 (1995), pp. 293–315.
- [21] S. F. COTTER, B. D. RAO, K. ENGAN, AND K. KREUTZ-DELGADO, *Sparse solutions to linear inverse problems with multiple measurement vectors*, IEEE Trans. Signal Process., 53 (2005), pp. 2477–2488.
- [22] B. E. DAHLBERG, C. E. KENIG, AND G. VERCHOTA, *Boundary value problem for the systems of elastostatics in Lipschitz domains*, Duke Math. Jour., 57 (1988), pp. 795–818.
- [23] M. E. DAVIES AND Y. C. ELDAR, *Rank awareness in joint sparse recovery*, IEEE Trans. Inf. Theory, 58 (2012), pp. 1135–1146.
- [24] D. L. DONOHO AND M. ELAD, *Optimally sparse representation in general (non-orthogonal) dictionaries via l_1 minimization*, Proc. Nati. Acad. Sci. USA, 100 (2003), pp. 2197–2202.
- [25] J. EOM, H. KANG, G. NAKAMURA, AND Y.-C. WANG, *Reconstruction of the shear modulus of viscoelastic systems in a thin cylinder: An inversion scheme and experiments*, Inverse Probl., 32 (2016), 095007.
- [26] G. ESKIN AND J. RALSTON, *On the inverse boundary value problem for linear isotropic elasticity*, Inverse Probl., 18 (2002), pp. 907–921.
- [27] B. S. GARRA, I. CESPEDES, J. OPHIR, S. SPRATT, R. A. ZUURBIER, C. M. MAGNANT, AND M. F. PENNANEN, *Elastography of breast lesions: Initial clinical results*, Radiology, 202 (1997), pp. 79–86.
- [28] G. GEYMONAT AND S. PAGANO, *Identification of mechanical properties by displacement field measurement: A variational approach*, Meccanica, 38 (2003), pp. 535–545.

- [29] J. F. GREENLEAF, M. FATEMI, AND M. INSANA, *Selected methods for imaging elastic properties of biological tissues*, Annu. Rev. Biomed. Eng., 5 (2013), pp. 57–78.
- [30] S. GUCHHAIT AND B. BANERJEE, *Anisotropic linear elastic parameter estimation using error in constitutive equation functional*, Proc. R. Soc. A, 472 (2016), 20160213.
- [31] K. M. HILTAWSKY, M. KRUGER, C. STARKE, L. HEUSER, H. ERMERT, AND A. JENSEN, *Freehand ultrasound elastography of breast lesions: Clinical results*, Ultrasound Med. Biol., 27 (2001), pp. 1461–1469.
- [32] M. IKEHATA, *Inversion formulas for the linearized problem for an inverse boundary value problem in elastic prospection*, SIAM J. Appl. Math., 50 (1990), pp. 1635–1644.
- [33] O. IMANUVILOV, G. UHLMANN, AND M. YAMAMOTO, *On uniqueness of Lamé coefficients from partial Cauchy data in three dimensions*, Inverse Probl., 28 (2012), 125002.
- [34] A. JIN, B. YAZICI, A. ALE, AND V. NTZIACHRISTOS, *Preconditioning of the fluorescence diffuse optical tomography sensing matrix based on compressive sensing*, Opt. Lett., 37 (2012), pp. 4326–4328.
- [35] J. M. KIM, O. K. LEE, AND J. C. YE, *Compressive MUSIC: Revisiting the link between compressive sensing and array signal processing*, IEEE Trans. Inf. Theory, 58 (2012), pp. 278–301.
- [36] T. Y. KIM, T. Y. KIM, Y. KIM, S. LIM, W. K. JEONG, AND J. H. SOHN, *Diagnostic performance of shear wave elastography for predicting esophageal varices in patients with compensated liver cirrhosis*, J. Ultrasound Med., 35 (2016), pp. 1373–1381.
- [37] O. K. LEE, H. KANG, J. C. YE, AND M. LIM, *A non-iterative method for the electrical impedance tomography based on joint sparse recovery*, Inverse Probl., 31 (2015), 075002.
- [38] O. K. LEE, J. M. KIM, Y. BRESLER, AND J. C. YE, *Compressive diffuse optical tomography: Non-iterative exact reconstruction using joint sparsity*, IEEE Trans. Med. Imag., 30 (2011), pp. 1129–1142.
- [39] O. LEE AND J. C. YE, *Joint sparsity-driven non-iterative simultaneous reconstruction of absorption and scattering in diffuse optical tomography*, Opt. Express, 21 (2013), pp. 26589–26604.
- [40] F. MONARD, *Taming unstable inverse problems: Mathematical routes toward high-resolution medical imaging modalities*, PhD Thesis, Columbia University, 2012.
- [41] G. NAKAMURA AND G. UHLMANN, *Global uniqueness for an inverse boundary problem arising in elasticity*, Invent. Math., 118 (1994), pp. 457–474.
- [42] G. NAKAMURA AND G. UHLMANN, *Erratum: Global uniqueness for an inverse boundary problem arising in elasticity*, Invent. Math., 152 (2003), pp. 205–207.
- [43] A. A. OBERAI, N. H. GOKHALE, S. GOENEZEN, P. E. BARBONE, T. J. HALL, A. M. SOMMER, AND J. JIANG, *Linear and nonlinear elasticity imaging of soft tissue in vivo: Demonstration of feasibility*, Phys. Med. Biol., 54 (2009), pp. 1191–1207.
- [44] K. J. PARKER, L. S. TAYLOR, S. GRACEWSKI, AND D. J. RUBENS, *A unified view of imaging the elastic properties of tissue*, J. Acoust. Soc. Am., 117 (2005), pp. 2705–2712.

- [45] R. SINKUS, J. LORENZEN, J. SCHRADER, M. LORENZEN, M. DARGATZ, AND D. HOLZ, *High-resolution tensor MR elastography for breast tumor detection*, Phys. Med. Biol., 45 (2000), pp. 1649–1664.
- [46] R. SINKUS, M. TANTER, T. XYDEAS, S. CATHELINE, J. BERCOFF, AND M. FINK, *Viscoelastic shear properties of in vivo breast lesions measured by MR elastography*, Magn. Reson. Imaging, 23 (2005), pp. 159–165.
- [47] R. SINKUS, J. BERCOFF, M. TANTER, J. L. GENNISSON, C. EL KHOURY, V. SERVOIS, A. TARDIVON, AND M. FINK, *Nonlinear viscoelastic properties of tissue assessed by ultrasound*, IEEE Trans. Ultrason., Ferroelectr. Freq. Control, 53 (2006), pp. 2009–2018.
- [48] A. TARANTOLA, *Inverse Problem Theory*, Elsevier, 1987.
- [49] A. WAHAB AND R. NAWAZ, *A note on elastic noise source localization*, J. Vib. Control, 22 (2016), pp. 1889–1894.
- [50] J. A. TROPP, *Algorithms for simultaneous sparse approximation. Part II: Convex relaxation*, Signal Process., 86 (2006), pp. 589–602.
- [51] A. B. WEGLEIN, F. V. ARAÚJO, P. M. CARVALHO, R. H. STOLT, K. H. MATSON, R. T. COATES, D. CORRIGAN, D. J. FOSTER, S. A. SHAW, AND H. ZHANG, *Inverse scattering series and seismic exploration*, Inverse Probl., 19 (2003), pp. R27–R83.
- [52] P. WELLMAN, R. H. HOWE, E. DALTON, AND K. A. KERN, *Breast tissue stiffness in compression is correlated to histological diagnosis*, Technical Report, Harvard BioRobotics Laboratory, Division of Engineering and Applied Sciences, Harvard University, 1999.
- [53] T. WIDLAK AND O. SCHERZER, *Stability in the linearized problem of quantitative elastography*, Inverse Probl., 31 (2015), pp. 035005.
- [54] D. P. WIPF AND B. D. RAO, *An empirical Bayesian strategy for solving the simultaneous sparse approximation problem*, IEEE Trans. Signal Process., 55 (2007), pp. 3704–3716.
- [55] D. P. WIPF, B. D. RAO, AND S. NAGARAJAN, *Latent variable Bayesian models for promoting sparsity*, IEEE Trans. Inf. Theory, 57 (2011), pp. 6236–6255.
- [56] J. C. YE AND S. Y. LEE, *Non-iterative exact inverse scattering using simultaneous orthogonal matching pursuit (S-OMP)*, in Proceedings of IEEE International Conference on Acoustics, Speech and Signal Processing (ICASSP 2008), Las Vegas, NV, 2008, pp. 2457–2460.